

# Metal Nanowire Networks: The Next Generation of Transparent Conductors

Shengrong Ye, Aaron R. Rathmell, Zuofeng Chen, Ian E. Stewart, and Benjamin J. Wiley\*

There is an ongoing drive to replace the most common transparent conductor, indium tin oxide (ITO), with a material that gives comparable performance, but can be coated from solution at speeds orders of magnitude faster than the sputtering processes used to deposit ITO. Metal nanowires are currently the only alternative to ITO that meets these requirements. This Progress Report summarizes recent advances toward understanding the relationship between the structure of metal nanowires, the electrical and optical properties of metal nanowires, and the properties of a network of metal nanowires. Using the structure–property relationship of metal nanowire networks as a roadmap, this Progress Report describes different synthetic strategies to produce metal nanowires with the desired properties. Practical aspects of processing metal nanowires into high-performance transparent conducting films are discussed, as well as the use of nanowire films in a variety of applications.

film comes from the slow (linear coating rate of ca.  $0.01 \text{ m s}^{-1}$ ), vapor phase sputtering process, which ensures that the cost of overhead per unit length of ITO film is high. In addition, more than 70% of the ITO sputtered from a target ends up on the walls of the sputtering chamber, from which it must be removed and recycled. Besides the need for a recycling infrastructure that does not add value, a major disadvantage of the sputtering process is that the rate of film throughput decreases with increasing film thickness, which makes thicker, high-conductivity ITO more expensive than low-conductivity ITO. Typical costs for ITO range from  $\$5.5 \text{ m}^{-2}$  for  $150 \Omega \text{ sq}^{-1}$  ITO, up to  $\$26 \text{ m}^{-2}$  for  $10 \Omega \text{ sq}^{-1}$  ITO.<sup>[5]</sup> The thickness-limited throughput of ITO is especially problem-

## 1. Introduction

Transparent conductors (TCs) are a necessary component in flat-panel televisions, e-readers, smart-phones, smart-glass, touch-screens, organic light emitting diodes (OLEDs), and organic photovoltaics (OPVs).<sup>[1]</sup> Indium tin oxide (ITO) is the most commonly used transparent conductor, with sales of approximately \$1.6 billion in 2013, or 93% of the entire market for transparent conductors.<sup>[2]</sup> The high transmittance (>90%) of ITO at low sheet resistances ( $10 \Omega \text{ sq}^{-1}$  on glass) is the primary reason for the popularity of ITO. However, there are several attributes of ITO that are undesirable.<sup>[3]</sup> ITO is a ceramic, and is thus brittle and prone to cracking. The abundance of indium in the earth's crust is low (0.05 ppm), and its cost is correspondingly high, approximately  $\$600 \text{ kg}^{-1}$ .<sup>[4]</sup> However, for a 100 nm-thick film of ITO, only approximately 2% of the cost can be attributed to the cost of raw indium.<sup>[5]</sup> Much of the cost of ITO

is especially problematic for OLEDs and solar cells due to the need for these devices to carry higher currents, and thus use relatively expensive ITO with a low sheet resistance (ca.  $10 \Omega \text{ sq}^{-1}$ ). For an OPV, ITO on polyethylene terephthalate (PET) can represent up to 51% of the materials cost.<sup>[6]</sup>

In contrast to vapor-phase coating processes, the speed of a solution-phase coating process does not necessarily have to decrease with increasing coating thickness.<sup>[7]</sup> Solution-phase coating processes also have lower capital and maintenance costs than sputtering.<sup>[6,8]</sup> These facts have motivated the search for alternatives to ITO that can be deposited from liquids at linear coating rates >100 times faster ( $>1 \text{ m s}^{-1}$ ) than the ITO sputtering process, but achieve the same or better transmittance and sheet resistance values. Given the fact that the cost of ITO is dominated by the cost of sputtering rather than the cost of indium, it seems sensible to focus our attention in this Progress Report on those alternatives to ITO that enable the replacement of sputtering with coating from solution.

Conducting polymers are one long-standing alternative to ITO that offer the ability to be printed from solution, as well as mechanical flexibility.<sup>[9]</sup> Poly(3,4-ethylenedioxythiophene) poly(styrenesulfonate) (PEDOT:PSS) is the most widely used conducting polymer for transparent electrodes, and often serves as the hole conducting layer between the active polymer and ITO in OLEDs and OPVs.<sup>[10]</sup> At a transmittance >90%, the typical sheet resistance values for PEDOT:PSS are  $>100 \Omega \text{ sq}^{-1}$ .<sup>[11]</sup> This performance is good enough for some applications that do not require high current carrying capacity, such as capacitive touch sensors and films that dissipate static electricity, but is not sufficient for replacement of ITO in OPVs and OLEDs.

Dr. S. Ye,<sup>[†]</sup> Dr. A. R. Rathmell,<sup>[†]</sup> Dr. Z. Chen,  
I. E. Stewart, Prof. B. J. Wiley  
Department of Chemistry  
Duke University  
NC 27708, USA  
E-mail: benjamin.wiley@duke.edu  
Dr. Z. Chen  
Department of Chemistry  
Tongji University  
Shanghai 200092, China



<sup>[†]</sup>These authors contributed equally to this work.

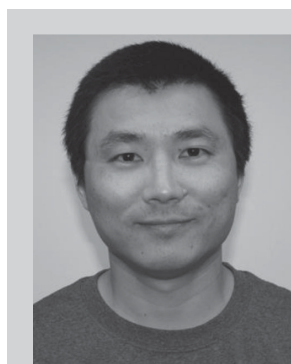
DOI: 10.1002/adma.201402710

Transparent, conducting networks of carbon nanotubes (CNTs) are a more recent alternative to ITO that are flexible, durable, and compatible with solution-phase roll-to-roll coating processes.<sup>[3,12]</sup> As-coated CNT-based transparent conductors typically exhibit sheet resistances of ca.  $400 \Omega \text{ sq}^{-1}$  at 90% *T* (% Transmittance) due to the large contact resistance between CNTs.<sup>[13]</sup> Through exfoliation/doping with chlorosulfonic superacid, Hecht et al. recently demonstrated a sheet resistance and transmittance of  $60 \Omega \text{ sq}^{-1}$  at 90.9%*T*, the highest optoelectronic performance to date for CNT films.<sup>[12c]</sup> Although this performance exceeds the performance of PEDOT:PSS, it is still about 5%*T* less than that of ITO at the same sheet resistance.

Graphene has electrical and optical properties that are similar to ITO when it is grown with a high temperature (1000 °C), chemical vapor deposition (CVD) process on a copper sheet, and transferred as one piece to a transparent substrate without damaging the atomically thin sheet.<sup>[14]</sup> However, this process as it stands is obviously not practical for production of a low-cost alternative to ITO. In contrast, films made by the solution-phase coating of graphene produced with low cost processes, such as exfoliating graphite, exhibit relatively poor performance (80%*T*,  $3 \text{ k}\Omega \text{ sq}^{-1}$ ).<sup>[15]</sup> This is likely due to the inherently low aspect ratio of graphene flakes and the high contact resistance between graphene sheets. It remains to be demonstrated whether it is possible to obtain ITO-level performance with solution-coated graphene.

Metals such as Ag, Cu, and Au are ca. 50 times more conductive than ITO, but continuous films of these metals are not very transparent. For example, a 7 nm film of Au exhibits a transmittance of 75% and a sheet resistance of  $20 \Omega \text{ sq}^{-1}$ ,<sup>[16]</sup> and a bilayer film of 7 nm Ag and 1 nm Ni has a sheet resistance of  $13 \Omega \text{ sq}^{-1}$  at a transmittance of 56%.<sup>[17]</sup> The performance of metal films can be improved dramatically by patterning them into grids with open holes that allow for the transmission of light. Indeed, several companies, including 3M, polyIC, Uni-Pixel, Kodak, O-film, and Atmel, offer or are working on microscale patterned metal grids as an alternative to ITO for use in touch sensors.<sup>[18]</sup> Although microscale patterned metal mesh offers optoelectronic performance comparable to or better than ITO, these films have yet to make much of a dent in the transparent conductor market. This may be because the cost of fabricating microscale metal grids ( $\$30\text{--}40 \text{ m}^{-2}$ ) is not substantially lower than the cost of ITO processing.<sup>[19]</sup> Metal grids cannot be used by themselves with OPVs or OLEDs due to the large (ca. 200  $\mu\text{m}$ ), non-conductive holes. The micron-scale surface roughness of the metal grids makes them incompatible with some types of OPV and OLED fabrication processes. The issues of hole size and surface roughness can be addressed to some extent for research purposes by replacing microscale grids made by photolithography and/or printing with nanoscale metal grids made with nanoimprint lithography techniques, but nanoscale patterning will likely introduce additional cost and suffer from lower yields.<sup>[20]</sup>

Fortunately, it is now possible to obtain a nanoscale metal mesh without any top-down patterning, and achieve performance equivalent to or better than ITO. This is possible by first growing metal nanowires in a scalable, solution-phase synthesis, transferring the nanowires into a coating medium, and coating the nanowires onto a transparent substrate. Cambrios



copper nanowires, to improve the control over their dimensions and properties.

**Shengrong Ye** (1979) was born in Shanghai, China. He received his Ph.D. degree in inorganic chemistry from West Virginia University in 2011, and is currently a postdoctoral research associate with Prof. Benjamin J. Wiley at Duke University. His research interests center on the mechanistic investigation of metal nanowires, especially



of various metal nanostructures and their incorporation into new and exciting devices.

**Aaron R. Rathmell** (1985) received his B.S. in Chemistry from Millersville University in 2008 and his Ph.D. in Chemistry from Duke University under the direction of Professor Benjamin J. Wiley in 2013. Currently Aaron is a post-doctoral researcher at EMD Millipore in Waltham, MA, USA. His research interests center on the synthesis



structures under the guidance of Prof. Younan Xia. Prior to joining Duke in 2009, he was a postdoctoral fellow in the laboratory of George Whitesides at Harvard University. His lab focuses on the processes by which atoms assemble to form nanostructures in solution, and the relationship between the structure and properties of these nanostructures in the context of practical applications.

**Benjamin J. Wiley** (1981) is an Assistant Professor in the Department of Chemistry at Duke University. He received his B.S. in Chemical Engineering from the University of Minnesota in 2003, and his Ph.D. in Chemical Engineering from the University of Washington in 2007, working on the synthesis of silver nanostructures

Technologies Corporation,<sup>[21]</sup> building upon a silver nanowire (Ag NW) synthesis developed in the lab of Prof. Younan Xia and licensed from the University of Washington, has refined and improved the synthesis, purification, and coating of Ag NWs to obtain films with a transparency of 95% at  $20 \Omega \text{ sq}^{-1}$ .<sup>[22]</sup> Even though silver (approximately  $\$765 \text{ kg}^{-1}$ ) is

**Table 1.** Comparison of transparent conducting materials in terms of their compatibility with solution coatable processes and performance relative to ITO.

TC Materials	Solution Coatable	ITO Level Performance	Examples
Doped Metal Oxides	No	Yes	Al:ZnO, <sup>[26]</sup> Ga:ZnO <sup>[27]</sup>
Metal Thin Films	No	No	Au, <sup>[16]</sup> Ag, <sup>[28]</sup> Ni, Cr <sup>[29]</sup>
Metal Nanogrids	No	Yes	Au, Ag, Cu <sup>[20b,30]</sup>
Electrospun Nanofibers	No	Yes	Cu <sup>[31]</sup>
Conductive Polymers	Yes	No	PEDOT:PSS <sup>[9b,10]</sup>
Carbon Nanotubes	Yes	No	[12b,12c,32]
Graphene Flakes	Yes	No	[15,33]
Metal Nanowires	Yes	Yes	Ag, <sup>[22]</sup> Cu <sup>[24a]</sup>

more costly than indium (approximately \$600 kg<sup>-1</sup>),<sup>[4,23]</sup> Ag NWs can be deposited from solution with low-cost, roll-to-roll slot die coating. Due to their lower processing costs, Ag NWs are being increasingly used as the transparent electrode in touch sensors for computers sold by LG and Lenovo.

Copper is only 6% less conductive than silver, but it is 1000-times more abundant and 100 times cheaper than silver or indium. Motivated by the potential to combine low-cost solution phase processing with the low cost of copper, several research groups have demonstrated scalable syntheses of copper nanowires (Cu NWs), as well as their coating from solution to make films with properties comparable to ITO.<sup>[24]</sup> The best sheet resistance and transmittance of Cu NW films demonstrated today are 100 Ω sq<sup>-1</sup> at 95%T.<sup>[24a]</sup> However, it remains a challenge to stabilize the Cu NWs against oxidation while retaining film performance comparable to ITO.

Of the various alternatives to ITO, only metal nanowires are both solution coatable and achieve performance equivalent to ITO (Table 1). In addition, metal nanowire films are not only much more flexible than ITO, but can even be made to be stretchable.<sup>[25]</sup> Thus metal nanowire films are currently the most promising material yet for replacing ITO across a broad range of existing and emerging applications. In this Progress Report, we summarize the rapid advances being made in the understanding of the structure–property relationship of metal nanowire films, as well as synthetic approaches to generating nanowires with structures specifically tuned for optimal performance in transparent, conducting nanowire networks. We then discuss different approaches to coat nanowires from solution and process the films to improve their conductivity, durability, and surface roughness. In the last section, we will highlight examples of the integration of transparent, conducting nanowire films into touch screens, OPVs, and OLEDs.

## 2. Structure–Property Relationships for Transparent Conducting Nanowire Films

How does the length and diameter of a metal nanowire affect the transmittance and sheet resistance of a transparent conducting film? A simple functional relationship between the

dimensions of a nanowire and the properties of the film would be very helpful in guiding synthetic efforts to produce nanowires that are optimized for use in transparent electrodes, but such a relationship does not currently exist. Obtaining such a relationship is complicated by the fact that: i) the intrinsic electrical and optical properties of metal nanowires are non-linearly dependent on nanowire diameter and ii) the dependence of the conductivity of nanowire films on the areal density and dimensions of nanowires cannot be solved analytically. In this section, we review current progress towards a complete, quantitative understanding of the structure–property relationship of nanowire films.

### 2.1. Size-Dependent Electrical Resistivity of Metal Nanowires

As the diameter of a metal nanowire becomes small relative to the mean free path of an electron, the electrical resistivity of the nanowire increases.<sup>[34]</sup> The first models for predicting how much the resistivity increases per decrease in dimension is attributed to Fuchs for the case of films;<sup>[35]</sup> Dingle extended this theory to metal wires.<sup>[34]</sup> These theories have been and continue to be attractive to experimentalists because they depend on only two parameters: i) the ratio of the sample dimension  $d$  to the bulk mean free path  $\lambda_\infty$  of an electron, and ii) an angle-independent specularly parameter  $p$  that gives the probability that an electron will be specularly reflected from the surface (i.e., not exhibit a decrease in drift velocity).

Recognizing that the reflection of a wave from a surface depends on the incident angle to and roughness of that surface (see Figure 1A), Ziman developed an angle and roughness-dependent specularly parameter of the form given by Equation 1:

$$p(\theta) = \exp \left[ - \left( 4\pi h / \lambda_e \right)^2 \cos^2 \theta \right] \quad (1)$$

where  $\theta$  is the angle of incidence relative to the surface normal,  $h$  is the root mean square surface roughness, and  $\lambda_e$  is the Fermi wavelength of an electron.<sup>[36]</sup> Soffer incorporated  $p(\theta)$  into a model for how the resistivity of thin films depends on surface roughness.<sup>[37]</sup> Sambles extended this theory to wires, and showed that this new model could better match and explain experimental results for thin films.<sup>[38]</sup> For example, to fit temperature-dependent experimental data with the Fuchs model, it proved necessary to introduce a temperature-dependent  $p$  or a temperature-dependent product of the bulk resistivity and the bulk mean free path,  $\rho_\infty \lambda_\infty$ , both of which have no physical basis. In contrast, the Soffer model shows excellent agreement with experimental data over a wide range of temperatures without requiring a temperature-dependent  $\rho_\infty \lambda_\infty$  to fit the data.

Given this long history of theoretical development, it is interesting to note that it is only within the last few years that experimental data has become available to test the Soffer–Sambles model of resistivity for nanowires. This is because testing this theory requires performing electrical measurements on nanowires with a roughness of about one tenth the Fermi wavelength of an electron, ca. 0.03 nm. Such experiments were recently performed by Kotov,<sup>[41]</sup> Peddetti,<sup>[40]</sup> and Krstic<sup>[39]</sup> for Au, Cu, and Ag NWs grown in solution-phase syntheses. Their

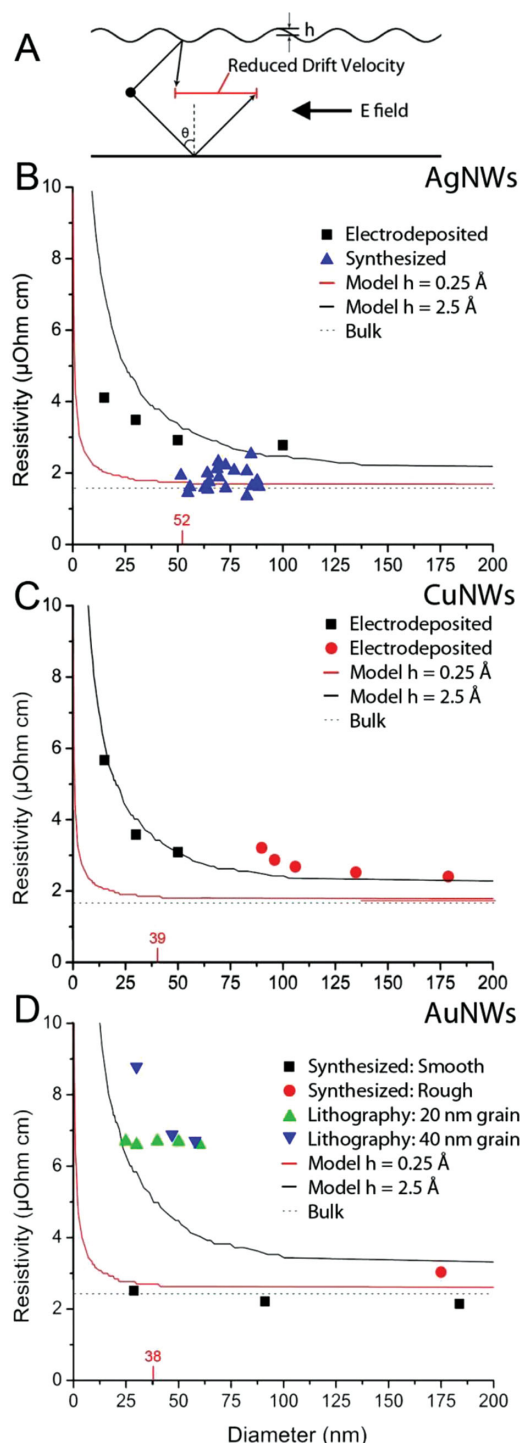


**Figure 1.** A) A schematic to illustrate the effect of surface roughness on the reflection of electrons from a surface. Plots of: B) Ag NWs,<sup>[39]</sup> C) Cu NWs,<sup>[40]</sup> and D) Au NWs<sup>[41]</sup> showing the experimental and theoretical (based on Samble's calculations) diameter-dependent resistivity. Data from the given references are plotted here. The red number on the x-axes shows the mean-free path for the various metals at room temperature.

data is plotted along with data from electrodeposited and lithographically-defined nanowires in Figure 1B–D. Model fits to the electrodeposited and lithographically-defined silver, copper, and

gold nanowires show that they are likely quite smooth, with a surface roughness of about 0.3 nm. However, this small surface roughness is still on the order of the Fermi wavelength of an electron (0.5 nm), and so these nanowires show enhanced resistivities at dimensions 2–6 times the bulk mean free path. In contrast, solution-grown Au and Ag NWs with atomically smooth surfaces exhibit resistivities comparable to the bulk, even at dimensions equivalent to or below the bulk mean free path of an electron.<sup>[39,41]</sup>

The recognition that atomically smooth metal nanowires exhibit very little enhancement in their resistivity is an exciting and important development for those working in the nanowire field. What this means for transparent conducting films is that one can utilize atomically smooth nanowires with smaller diameters without significantly degrading the resistivity of the film if the atomically smooth surfaces of the nanowires are retained after incorporation into devices. To come to a fuller understanding of the impact of nanowire diameter on the electro-optical performance of transparent conducting films, we will now examine the optical properties of nanowires.

## 2.2. The Optical Properties of Nanowire Films

The optical properties of a nanowire network can be understood by first considering what fraction of the surface of an otherwise transparent film is blocked by the nanowires. If the amount of light blocked by a single nanowire is equivalent to its geometric cross-section, then the light blocked by a nanowire network is approximately the area fraction ( $AF$ ) of the film covered by the nanowires, given by Equation 2:

$$AF = N \times L \times D \quad (2)$$

where  $N$  is the number of nanowires per unit area,  $L$  is the length of the nanowires, and  $D$  is the diameter of the nanowires.<sup>[42]</sup> The amount of light blocked by a single nanowire can be described by its extinction efficiency  $Q_{\text{ext}}$ , given by Equation 3:

$$Q_{\text{ext}} = \frac{C_{\text{ext}}}{DL} \quad (3)$$

where  $C_{\text{ext}}$  is the extinction cross-section of a nanowire, i.e., the amount of light scattered and absorbed by a nanowire.  $Q_{\text{ext}}$  is essentially the ratio of the amount of light scattered and absorbed by a nanowire relative to its geometric cross-section. The amount of light blocked by a nanowire film is then just  $AF \times Q_{\text{ext}}$ , and its transmittance (% $T$ ) is given by Equation 4:

$$\%T = e^{-AF \times Q_{\text{ext}}} \quad (4)$$

For nanowires more than several microns long, the  $Q_{\text{ext}}$  of a nanowire is independent of nanowire length,<sup>[42]</sup> and the diameter-dependent  $Q_{\text{ext}}$  of a nanowire can be calculated with Mie theory.<sup>[43]</sup> Figure 2A shows a plot of % $T$  at  $\lambda_0 = 600$  nm versus  $Q_{\text{ext}}$  for nanowires with diameters of 56, 100, and 153 nm. This data illustrates that the slope of a plot of % $T$  versus  $AF$  is linear with a diameter-dependent slope given by  $Q_{\text{ext}}$ . The slopes of the experimental measurements match the slopes calculated



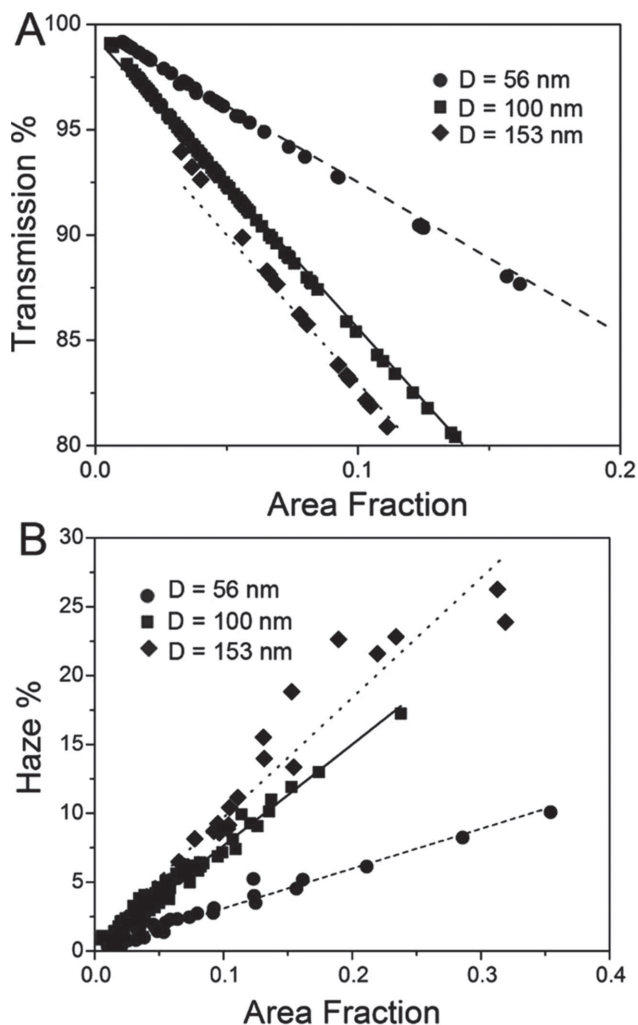


**Figure 2.** A) Optical transmission and B) haze versus area fraction of Ag NWs with a diameter of 56, 100, and 153 nm. Reproduced with permission.<sup>[43]</sup> Copyright 2013, AIP Publishing.

by Mie theory (dotted lines). Ag NWs with large diameters are more efficient at blocking light than nanowires with smaller diameters due to their larger extinction cross-sections.

Another important optical property of transparent conducting films is haze. Haze is defined as the percentage of transmitted light which in passing through the film deviates more than  $2.5^\circ$  from the incident beam by forward scattering, given by Equation 5:<sup>[44]</sup>

$$H = \frac{(I_s)_{2.5^\circ-90^\circ}}{I_d + (I_s)_f} \quad (5)$$

where  $I_d$  is the light flux transmitted directly, and  $(I_s)_f$  is the flux undergoing forward scattering, i.e. the scattered intensity between  $0^\circ$  and  $90^\circ$ . Minimizing haze, and thereby improving the clarity of a film, is an important consideration for display applications. Generally the haze of a touch screen should be less than 1%. In contrast, one may wish to increase haze for the transparent electrode in a solar cell, as an increase in the percent of light scattered from the electrode can increase

the coupling of light into the absorber material, and thereby increase the efficiency of the device.<sup>[43,45]</sup> Figure 2B shows the haze of a nanowire film as a function of AF for three diameters of nanowires. Haze increases roughly linearly with AF, and decreases exponentially with the diameter of the nanowires due to the decrease in the scattering cross-section.

### 2.3. The Electrical Properties of Nanowire Films

Given that the transmittance of a nanowire film decreases with the nanowire diameter  $D$  and area fraction  $AF$ , optimizing the optoelectronic properties of nanowire films requires minimizing the sheet resistance at a given  $D$  and  $AF$ . Of course, for a nanowire film to be electrically conductive at all, the nanowires must first be in contact. Imagine adding nanowires to a surface between two electrodes. At some critical nanowire number density  $N_c$ , one continuous path along interconnected nanowires is formed between the electrodes, and electrons can percolate across this path. Pike and Seager used Monte Carlo simulations to show that for wires of length  $L$  the critical number density  $N_c$  necessary to achieve percolation is given by Equation 6:<sup>[46]</sup>

$$N_c L^2 = 5.71 \quad (6)$$

This equation illustrates that it is important to use long nanowires in order to achieve a conducting path at low nanowire densities. Thus, in order to maximize the number of connections between nanowires at a low area fraction, it is necessary to maximize  $L/D$ , the aspect ratio of the nanowires.

However, most practical applications require nanowire networks with densities well above percolation, such that the nanowires in the film are all interconnected. At this point, the sheet resistance of a randomly oriented nanowire network is a function of the nanowire resistivity (which can in turn be a function of their diameter and surface roughness), the nanowire length  $L$ , the nanowire diameter  $D$ , the area fraction  $AF$  of nanowires, and the contact resistance between the nanowires. If the resistivity of the nanowires in a film is the same as the bulk resistivity  $\rho_{NW}$ , and the contact resistance  $R_c$  between the nanowires is negligible, then the sheet resistance of a nanowire film is given by Equation 7:

$$R_s = \frac{\rho_{NW}}{m/A} \quad (7)$$

where  $R_s$  ( $\Omega \text{ sq}^{-1}$ ) is the sheet resistance of the film (i.e., the resistance across a square-shaped area of the film),  $m/A$  ( $\text{kg m}^{-2}$ ) is the mass of the nanowires per unit area,  $\rho_{NW}$  ( $\text{kg m}^{-3}$ ) is the density of the nanowires in the film, and  $\rho_{NW}$  ( $\Omega \text{ m}$ ) is the bulk resistivity of the metal. Note that by neglecting contact resistance, the deviation of  $R_s$  from the sheet resistance of a solid metal film simply becomes a function of the porosity of the nanowire film,  $\rho_{NW}/\rho_B$ , where  $\rho_B$  is the bulk density of the metal.

However, the assumption that the contact resistance  $R_c$  is negligible is not a good assumption. In fact, experimental results indicate that it is better to assume that  $R_c \gg R_{NW}$ , where  $R_{NW}$  is the resistance of an individual nanowire. For example, electrical measurements of crossed Ag NWs with average diameters

$D \approx 40\text{--}80\text{ nm}$  are ca.  $8\text{ k}\Omega$  for plasmonically welded junctions<sup>[47]</sup> and ca.  $0.5\text{ k}\Omega$  for Ag NWs coated with gold.<sup>[48]</sup> In contrast, assuming the nanowire resistivity is the same as the bulk, the resistance of a Ag NW  $50\text{ nm}$  in diameter and  $10\text{ }\mu\text{m}$  long is  $0.08\text{ k}\Omega$ . The assumption that  $R_c \gg R_{NW}$  has (at least) three important implications: i) lowering the sheet resistance of a nanowire film at a given AF requires either reducing the number of contacts or reducing the contact resistance; ii) the number of contacts, and thus  $R_s$ , for a nanowire film at a given AF can be reduced by increasing the aspect ratio  $L/D$  of nanowires; iii) the  $R_s$  of a nanowire film will always depend on  $L/D$ , even for thick nanowire films in which the nanowires are all interconnected.

Calculations of the sheet resistance of nanowire networks as a function of AF and  $L/D$  for the case of  $R_c \gg R_{NW}$  by Mutiso et al. have not only quantitatively demonstrated the effects of  $R_c$  dominating the resistance of the film, but further show that this

assumption yields an excellent fit with experimental data.<sup>[49]</sup> To calculate the  $R_s$  of nanowire networks, random assemblies of ca.  $1000\text{--}450\,000$  nanowires were generated within a square cell with a thickness  $D$  (the nanowires are interpenetrating), and the network(s) of interconnected nanowires that span the breadth of the cell are identified. Assuming that all the resistance in the nanowire network comes from the contact resistance  $R_c$  between the nanowires, the current for a given bias across the cell is calculated by solving the system of equations that results from applying Kirchhoff's law to each nanowire junction. The sheet resistance of the cell is then calculated from the current across the cell for a given voltage, and the cell dimensions. Simulated  $R_s$  values can be fit to experimental  $R_s$  values by adjusting the one free parameter in the simulation,  $R_c$ . This approach allows one to extract the effective contact resistance  $R_{c\_effective}$  (See Figure 3A) between a large number of diverse

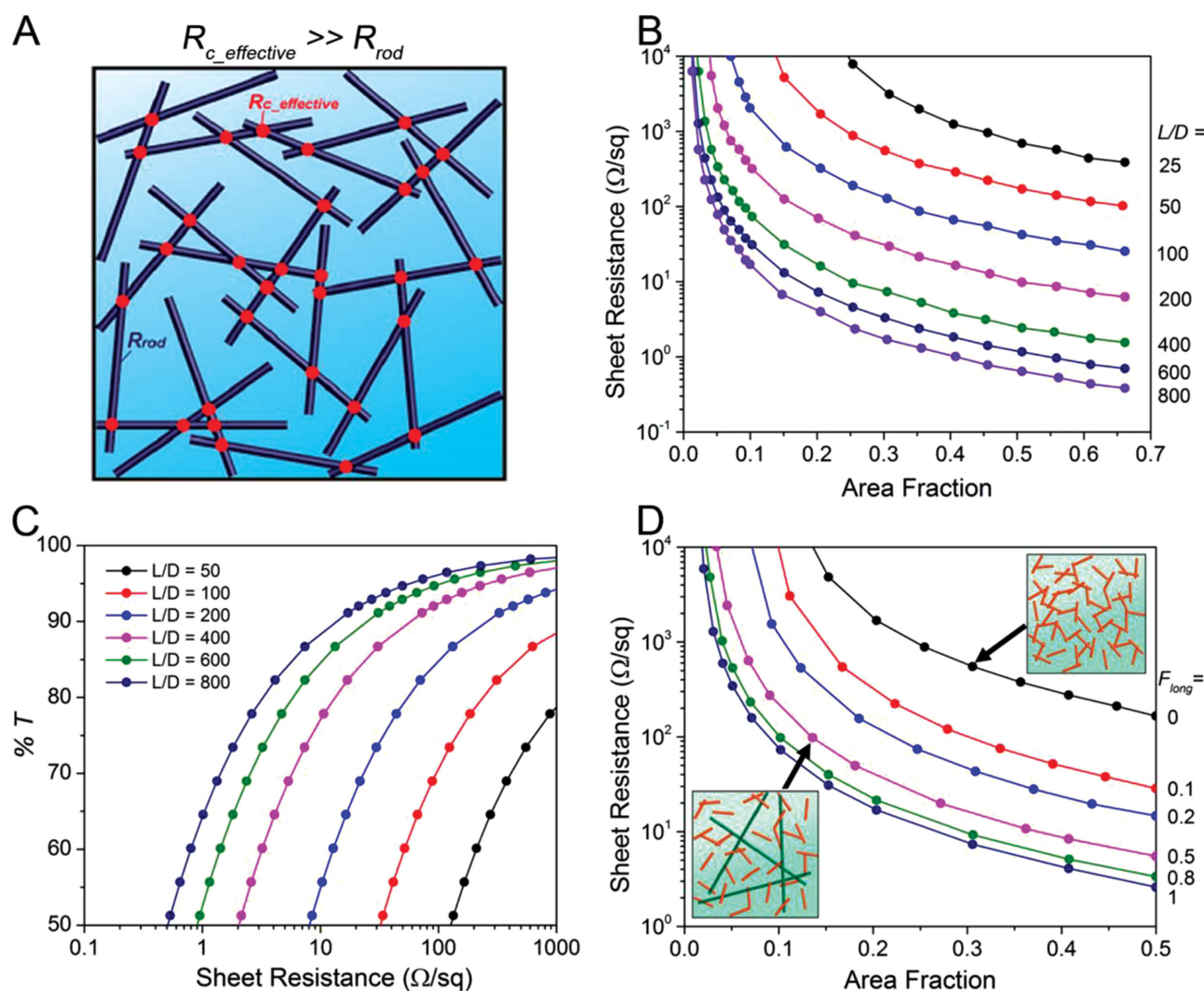


**Figure 3.** A) A schematic of a network of monodisperse nanowires in which the resistance at nanowire–nanowire junctions (red dots) dominates ( $R_c \gg R_{NW}$ ). B) Sheet resistance from simulations as a function of the  $L/D$  and area fraction of the rods in Ag NW films using an effective average contact resistance  $R_{c\_effective} = 2\text{ k}\Omega$  and constant  $D = 50\text{ nm}$ . C) Calculated transmittance vs simulated sheet resistance for Ag NW films for  $L/D$  ranging between 50 and 800. D) Simulated sheet resistance as a function of area fraction for nanowire films composed of bidisperse mixtures of rods with  $L/D = 50$  (Reference) and 400 (Long). Insets are schematics illustrating networks with different relative area fractions of long rods in the network,  $F_{Long} = 0$  (upper right) and  $F_{Long} = 0.5$  (lower left). Reproduced with permission.<sup>[49]</sup> Copyright 2013, American Chemical Society.

nanowire junctions in an experimental nanowire network. For Ag NWs with  $D = 50\text{--}80\text{ nm}$ ,  $R_{\text{c, effective}} = 1.5\text{--}2.5\text{ k}\Omega$ . This value falls within the range of individual Ag NW junctions that were measured experimentally ( $0.5\text{--}8\text{ k}\Omega$ ).

After obtaining a value of  $R_{\text{c, effective}} = 2\text{ k}\Omega$  from fits with experimental Ag nanowire networks ( $D = 50, 84, \text{ and } 75\text{ nm}$ ;  $L/D = 200, 258, \text{ and } 275$ ), the simulation allowed for the rapid calculation of  $R_s$  values across a broad range of  $L/D$  and  $AF$  values. Figure 3B demonstrates the strong dependence of  $R_s$  on aspect ratio for nanowire networks with  $R_c \gg R_{\text{NW}}$ , even for dense networks with  $AF = 0.7$ . For dense networks, the  $R_s$  drops by a factor of ca. 4 for every doubling of  $L/D$  at a given area fraction, and thus continues to obey the  $L^{-2}$  scaling predicted by percolation theory for networks near the critical density required for percolation. Figure 3C combines the  $R_s$  calculation with empirical fits for  $\%T$  as a function of  $AF$  to demonstrate how the  $\%T$  and  $R_s$  scale with aspect ratio. This plot clearly shows that it is necessary to use high aspect ratio nanowires in order to obtain high performance transparent conducting films. It also shows that it is important for experimentalists to report the aspect ratio of the nanowires they used for a given film so as to facilitate the comparison of results between research groups.

Of course, synthesized nanowires consist of a range of aspect ratios, so it is important to understand the effect of this distribution of aspect ratios on the properties of a nanowire network. Figure 3D shows the effect of replacing a given area fraction of short nanowires ( $L/D = 50$ ) with long nanowires ( $L/D = 400$ ). The  $R_s$  of the network drops by nearly an order of magnitude when only 10% of the area fraction of short nanowires is replaced by long nanowires. This positive result suggests that the longer nanowires in a sample with a large range of nanowire aspect ratios will have a much stronger effect on the film performance than the nanowires with low aspect ratios. The schematics in Figure 3D illustrate that adding a small proportion of high aspect ratio nanowires allows electrons to traverse much farther across a film without encountering a high-resistance nanowire contact.

### 3. Scalable Synthesis of Metal Nanowires

The fact that metal nanowires can be grown in liquid solutions at low temperatures makes them particularly easy to commercialize because solution-phase syntheses are orders of magnitude less capital-intensive and easier to scale than vapor-phase processes. It is remarkable to note that methods for the solution-phase growth of metal nanowires without a template did not exist fifteen years ago, but now there are hundreds of different syntheses for producing metal nanowires in solution and a dozen companies producing and selling metal nanowires for a variety of applications. All solution-phase syntheses of nanowires are similar in that they require a reducing agent to convert metal ions into metal and a capping agent to direct anisotropic assembly of the metal atoms into nanowires. In this section, we will highlight some of the synthetic processes capable of producing metal nanowires from silver and copper with lengths, widths, and yields well-suited for use in transparent conducting films.

#### 3.1. Silver Nanowires

The polyol synthesis of Ag NWs developed by Sun, Xia and co-workers in 2002 represents one of the earliest syntheses suitable for scalable production of metal nanowires, and variations of it are widely used for commercial production of Ag NWs for transparent conducting films.<sup>[50]</sup> This synthesis involves the reduction of silver ions by hot ethylene glycol (EG) in the presence of polyvinylpyrrolidone (PVP), a polymeric capping agent (Figure 4A). Typically the EG is preheated to the desired temperature (ca.  $150\text{ }^\circ\text{C}$ ) before adding solutions containing the

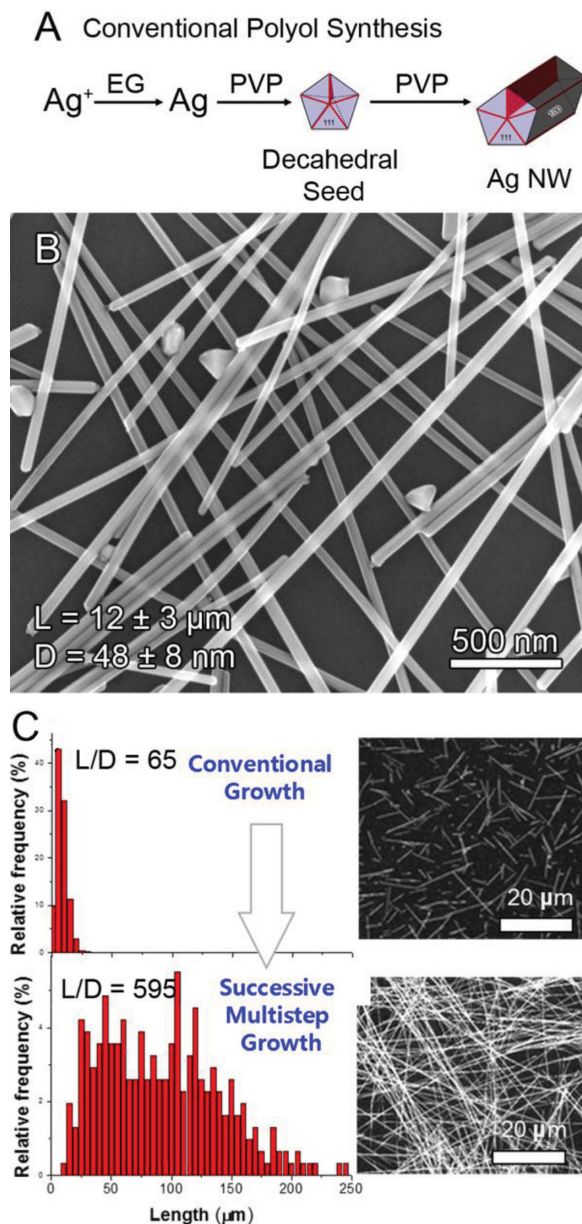


**Figure 4.** A) Conventional polyol synthesis of Ag NWs. B) SEM image of the Ag NWs. C) Length distributions of Ag NWs from conventional growth and successive multistep growth and their corresponding SEM images. Reproduced with permission.<sup>[51]</sup> Copyright 2012, The Royal Society of Chemistry.



dissolved silver precursor (usually  $\text{AgNO}_3$ ) and PVP (a molecular weight of 55 000 seems to work best).

Heating of the ethylene glycol generates glycolaldehyde, which in turn reduces the silver ions to atoms. The atoms then agglomerate to form nuclei. At a small size, the crystal structure of the nuclei will fluctuate between a single-crystalline, single-twinned, or a multiply twinned decahedral morphology.<sup>[52]</sup> As the nuclei grow, the amount of energy required to break the bonds in the nuclei and modulate its morphology becomes greater than the thermal energy available. At this point the nuclei become stuck in a given morphology, and are then called seeds. Generally a high-yield of the multiply twinned seeds are observed due to the ability of twinning to increase the coverage of the lowest-surface-energy, (111) facets.<sup>[53]</sup> Silver atoms preferentially add to the faces of the decahedra, leading to their elongation into nanorods. PVP is then thought to preferentially adhere to the sides of the nanorods, leaving their ends open to further atomic addition.<sup>[54]</sup> This leads to the rapid anisotropic growth of nanorods into nanowires.

For consistently high yields of high-aspect-ratio Ag NWs, the starting EG should contain very low concentrations of Fe and Cl species, which are common contaminants. One source for high purity EG is J. T. Baker, which conveniently puts the lot analysis for Cl and Fe on the label. Before using the EG in the reaction, it must be doped with a controlled amount of Fe and Cl (for example, with about 5  $\mu\text{M}$  of  $\text{Fe}(\text{NO}_3)_3$  and 0.22 mM of NaCl).<sup>[42]</sup> If no  $\text{Cl}^-$  is added, the silver seeds will rapidly agglomerate into spheroids. Although it is not entirely clear how the Cl anions prevent aggregation of seeds, one possibility is that the Cl anions coordinate to the surface of the seeds, imbue them with negative charge, and thus electrostatically stabilize them against aggregation. However, if the reaction is performed in air, the coordination of Cl anions to the silver decahedra will also assist in their oxidative dissolution. One way to prevent this is to add Fe(III) cations. Although it is again not entirely clear how a small amount of Fe(III) can prevent oxidative dissolution, one possibility is that reduction by glycolaldehyde keeps the iron species in the divalent state, and these divalent iron species act as oxygen scavengers.<sup>[55]</sup>

A typical polyol synthesis produces Ag NWs 2–25  $\mu\text{m}$  long and 40–90 nm wide, with  $L/D = 50$ –300 (Figure 4B). As mentioned in the discussion above, it would be beneficial to synthesize nanowires that have higher aspect ratios and smaller diameters. Previous work has shown that the reducing power of EG increases with temperature, and that this effect is due to the temperature-dependent oxidation of ethylene glycol to glycolaldehyde.<sup>[56]</sup> Therefore, the reaction temperature and time will affect the growth rate, and thereby determine the dimension of the nanowires. However, it is challenging to produce nanowires with aspect ratios  $>400$  or diameters  $<30$  nm only by controlling the time and temperature of a polyol synthesis.<sup>[42]</sup>

Recently Ko and co-workers have developed a successive multistep growth method using the as-synthesized nanowires as “seeds” for growing longer nanowires (Figure 4C).<sup>[51]</sup> In this method a modified  $\text{CuCl}_2$ -mediated polyol process was used to synthesize the starting nanowires (ca. 10  $\mu\text{m}$ ).<sup>[57]</sup> The as-synthesized nanowires were then used as seeds to grow nanowires in a fresh growth solution containing EG, PVP, and  $\text{AgNO}_3$  at 150  $^\circ\text{C}$ . To further increase the length of the nanowires, this

process was repeated several times on the same nanowires. As shown in Figure 4C, seven iterations of this produced nanowires as long as 500  $\mu\text{m}$  with an average diameter of 160 nm ( $L/D = 600$ ). Although the aspect ratio of these nanowires is fairly high, their large diameters will give these nanowire large extinction cross-sections. In addition, the successive growth method is not a practical method for large-scale production of silver nanowires. There remains a gap in the literature for silver nanowire syntheses that produce high aspect ratio nanowires with diameters less than 30 nm.

### 3.2. Copper Nanowires

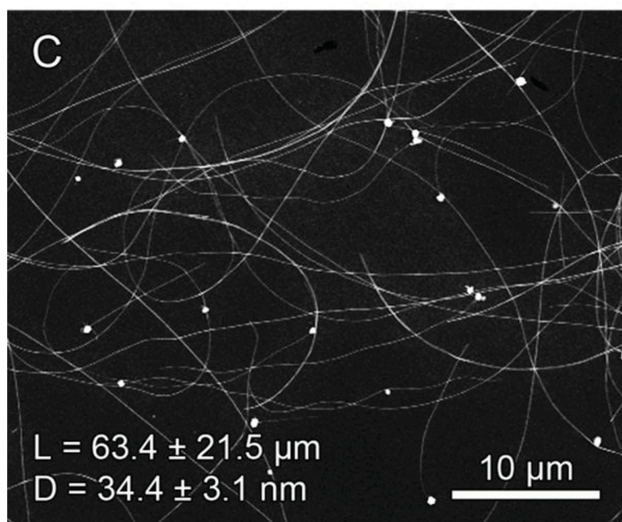
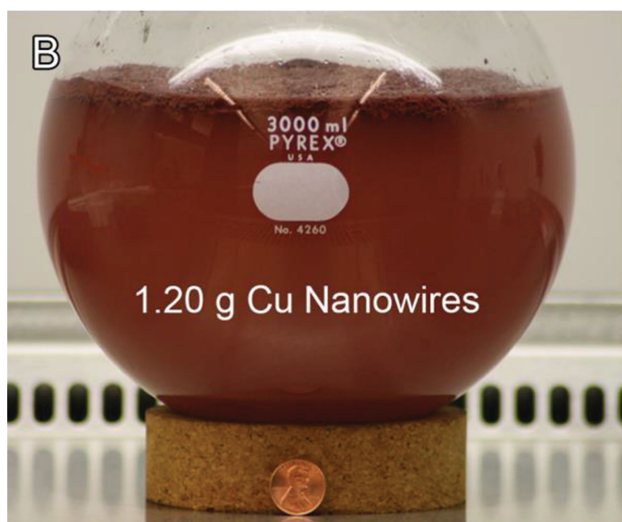
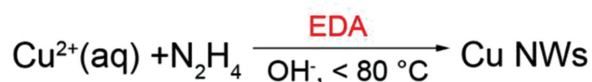
Several Cu NW syntheses have been published over the past decade, but there are two general approaches that are used by multiple labs: i) an ethylenediamine (EDA)-mediated synthesis, and ii) an alkylamine-mediated synthesis. Zeng and co-workers developed one of the first scalable solution phase synthesis of Cu NWs in 2005 (Figure 5A).<sup>[58]</sup> In this synthesis, Cu(II) ions are reduced by hydrazine ( $\text{N}_2\text{H}_4$ ) in a basic solution (pH = 14–15) containing EDA as the capping agent. The resulting Cu NWs were 90–120 nm in diameter and 40–50  $\mu\text{m}$  long ( $L/D = 350$ –450). Rathmell et al. modified Zeng's approach and scaled the reaction up by 100 times (1.2 g Cu NWs) to demonstrate the potential for large scale production (Figure 5B).<sup>[24b]</sup> The Cu NWs were  $90 \pm 10$  nm wide and  $10 \pm 3$   $\mu\text{m}$  long with spherical nanoparticles attached to one end of the nanowires. The addition of EDA to the reaction solution was necessary to promote anisotropic growth of Cu NWs. Without EDA added to the reaction, only particles with diameters ranging from 125–500 nm were produced. Ye et al. increased the aspect ratio of the Cu NWs up to 2300 (80  $\mu\text{m}$  long and 35 nm wide) by modifying the EDA-mediated approach (Figure 5C).<sup>[24a,59]</sup> They found the size and shape of the Cu NWs were controllable through adjustment of the molar ratio of  $\text{Cu}(\text{NO}_3)_2$ ,  $\text{N}_2\text{H}_4$ , and EDA.

The alkylamine-mediated synthesis is usually carried out in a neutral or moderately basic condition at a higher temperature than the EDA-mediated synthesis (Figure 5D). Shi et al. reported a hydrothermal route to obtain Cu NWs by reducing  $\text{CuCl}_2$  in water at 120–180  $^\circ\text{C}$ .<sup>[60]</sup> In this method, octadecylamine reduced Cu(II) to Cu(0) and served as a capping agent. The Cu NWs produced by this method had diameters of 30–100 nm and lengths up to several millimeters. Peng and co-workers replaced the octadecylamine with oleylamine, and introduced Ni(II) as a catalyst for reduction of Cu(II).<sup>[24f]</sup> These modifications reduced the average diameter of the Cu NWs below 16 nm, and the lengths were up to 40  $\mu\text{m}$  ( $L/D < 2500$ ). Konya and co-workers introduced an additional reducing agent, glucose, to the alkylamine-mediated synthesis of Cu NWs, which enabled the use of lower reaction temperatures (120  $^\circ\text{C}$ ).<sup>[61]</sup> The Cu NWs had a uniform diameter of 65 nm and a length of a few micrometers ( $L/D > 50$ ). Xia and co-workers reduced the temperature of the hexadecylamine/glucose reaction to 100  $^\circ\text{C}$  to produce Cu NWs with an average diameter of 25 nm and a length ranging from tens to hundreds of micrometers (Figure 5E,F).<sup>[24c]</sup>

At the present time, both the EDA-mediated and alkylamine-mediated synthesis can produce thin, high-aspect-ratio



## A EDA-Mediated Synthesis



## D Alkylamine-Mediated Synthesis

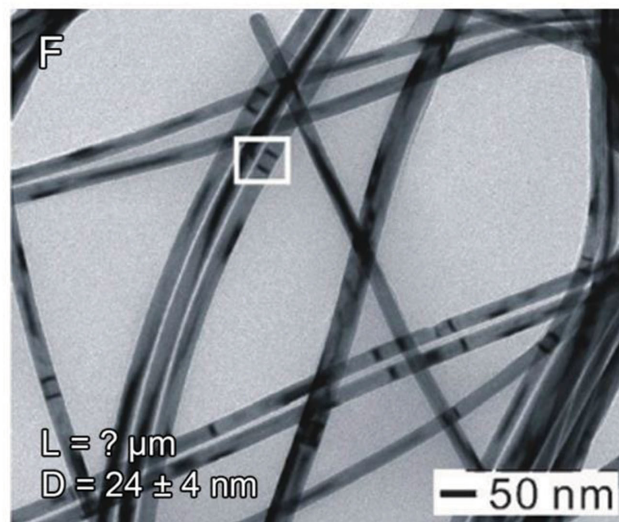
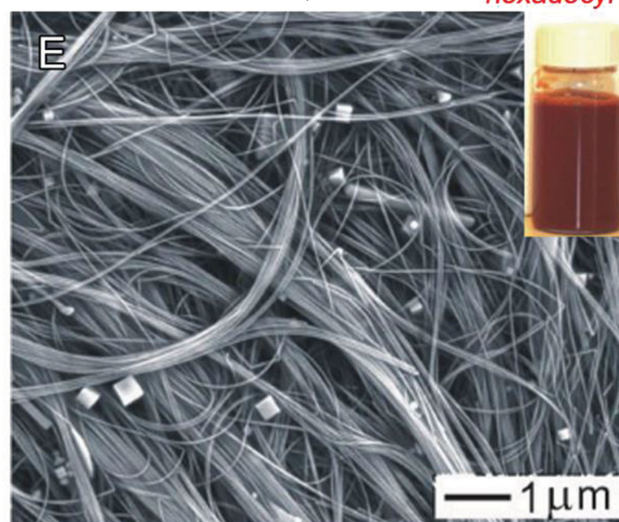
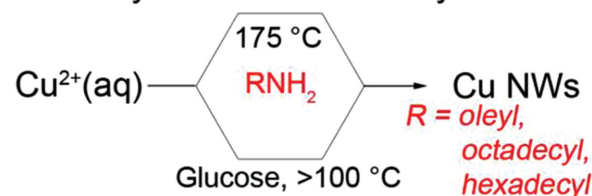


**Figure 5.** A) Reaction scheme of EDA-mediated synthesis. B) Picture of the reaction flask after growth of Cu NWs at 80 °C for 1 hr. Reproduced with permission.<sup>[24b]</sup> Copyright 2010, Wiley-VCH. C) SEM image of Cu NWs. Reproduced with permission.<sup>[24a]</sup> Copyright 2014, Royal Society of Chemistry. D) Reaction scheme of alkylamine-mediated synthesis. E,F) SEM (E) and TEM (F) images of Cu NWs prepared with hexadecylamine as capping agent. The inset in (E) shows the as-prepared suspension of Cu NWs in water. Reproduced with permission.<sup>[24c]</sup> Copyright 2011, Wiley-VCH.

nanowires that have equally good performance when processed to form transparent conducting films.<sup>[24a,24d–f,59,62]</sup> Although the EDA-mediated synthesis is carried out under very basic conditions, the fact that it can be performed under atmospheric pressures makes it more practical for large-scale production. **Figure 6** shows the best transmittance and sheet resistance reported in the literature to date for solution-coated Ag NWs, Cu NWs, graphene, CNTs and PEDOT:PSS.

#### 4. Film Fabrication

A variety of coating methods have been employed to fabricate transparent conductors made from metal nanowires, including drop casting, vacuum filtration, spin coating, spray coating, and Meyer rod coating. Drop casting<sup>[64]</sup> involves dropping and drying a volume of nanowire suspension on a substrate that is agitated on a shaker. The resulting nanowire mesh can be

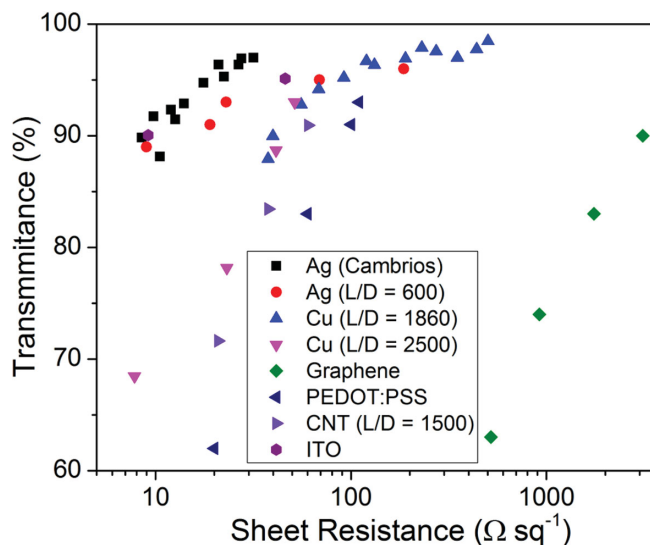


**Figure 6.** Plot of specular transmittance versus sheet resistance for the best available Ag NW ( $L/D = 600$ ,<sup>[51]</sup> Cambrios)<sup>[22]</sup> and Cu NW ( $L/D = 1860$ ,<sup>[24a]</sup> 2500)<sup>[24f]</sup> transparent conducting films. Values for CNT,<sup>[12c]</sup> graphene,<sup>[63]</sup> and PEDOT:PSS<sup>[10,11]</sup> based films, and ITO are shown for comparison. Data from the given references are plotted here.

randomly dispersed in the center of the droplet but often forms a coffee ring of dense wires around the edge of the droplet. More uniform nanowire films can be formed on a filter membrane using vacuum filtration.<sup>[24b,24e,24f,25f,42,51,65]</sup> This film can then be transferred to various substrates including glass, polydimethylsiloxane (PDMS), and PET. This method is particularly good for producing films with a known area fraction of nanowires by filtering a solution with a known nanowire concentration. Of course, this method is not scalable, and it can be challenging to completely transfer the nanowires from the filter to a substrate. Spin coating<sup>[66]</sup> requires the placement of excessive amounts of nanowire suspension on a flat substrate, followed by rotation at high speeds to spread the nanowire solution evenly across the substrate through centrifugal force. The area fraction of the nanowire films can be adjusted by varying the spin rate and the concentration of the nanowire suspension. This process can be convenient for quickly checking a sample in a laboratory setting, but is obviously not very scalable.

Random networks of nanowires can also be sprayed from dilute suspensions using an airbrush or electrostatic spray deposition.<sup>[25e,67]</sup> This method sometimes requires that the substrate to be heated to evaporate the solvent, especially if the solvent is water. The spray pressure can be adjusted to produce small droplets to improve the uniformity of the film.<sup>[67g]</sup> Spray coating is particularly well-suited for applying nanowires to curved and irregularly shaped surfaces.

Meyer rod coating is a simple and scalable method to make transparent films of metal nanowires.<sup>[24a,24d,48,59,62a,62b,68]</sup> Ag NWs can be coated directly from methanol or other alcohols (Figure 7A).<sup>[48,68a-c]</sup> A nitrocellulose-based ink was developed for Meyer rod coating of Cu NWs.<sup>[24a,24d,59,62a,62b,62d,62e]</sup> Meyer rod coating is more scalable than spray coating as it enables faster deposition of nanowires to the film.

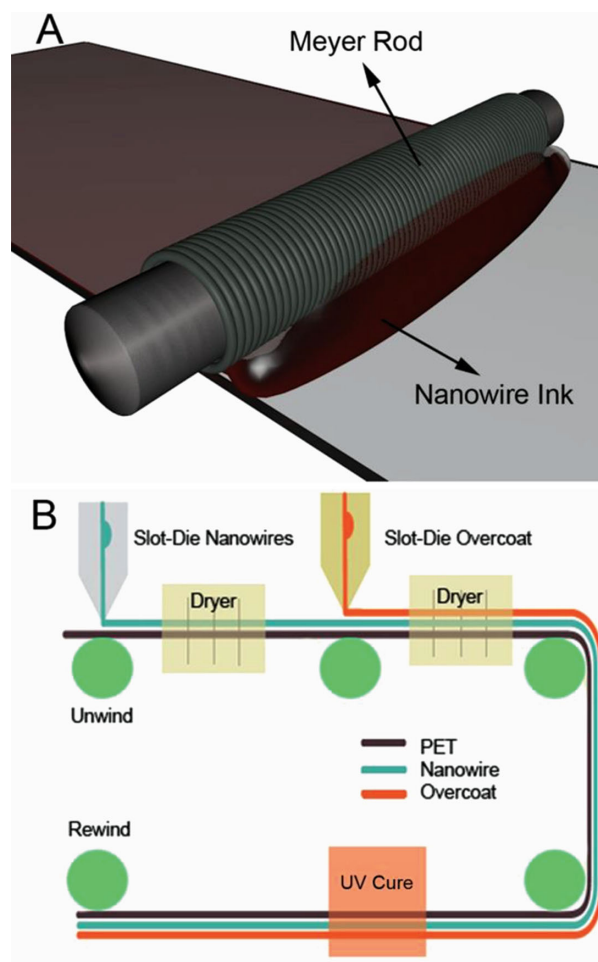


**Figure 7.** A) Meyer rod coating and B) roll-to-roll slot die coating.

Cambrios has reported the ability to create highly transparent conducting films consisting of Ag NWs using roll-to-roll slot-die coating on plastic substrates.<sup>[21]</sup> A conceptual schematic on the Ag NW film production process is shown in Figure 7B. An aqueous dispersion of Ag NWs are coated and dried on a PET film, followed by a thin (100–150 nm), transparent, UV-curable polymer overcoat. The purpose of the overcoat layer is to impart mechanical strength to the coating, and protect the nanowire layer from direct environmental exposure. All processing steps can be performed at low temperatures (<120 °C) and are thus compatible with most types of optical grade plastic film such as PET, polycarbonate, triacetyl cellulose, or cyclic olefin polymer. The wet-film thickness, and thus, the conductivity and transmittance of the nanowire films, can be tuned by adjusting the roll-to-roll coating parameters or the concentration of the nanowire ink without compromising the coating throughput.

## 5. Post-Treatment

Polymers or oxides on the surface of the nanowires after the coating step may increase the contact resistance between the nanowires in a network. The nanowire film is also fairly rough

compared to ITO, can usually be wiped off the substrate with a finger, and is susceptible to corrosion. In the following section, we will present a variety of methods to render nanowire films more conductive, smooth, mechanically robust, and corrosion resistant.

### 5.1. Reduction of Wire–Wire Contact Resistance

As we noted in Section 2.3, the majority of the sheet resistance of a nanowire film arises from the contact resistance between nanowires. It is therefore critical to minimize contact resistance between nanowires in order to lower the sheet resistance of a nanowire network. Lowering the contact resistance between nanowires requires increasing the metallic contact area between nanowires and removing barriers to electron transport. There

are several ways to achieve this. Thermal annealing of the Ag NW networks at a temperature of 200 °C for 20 min resulted in a dramatic decrease in the sheet resistance from 1 k $\Omega$  sq<sup>-1</sup> to 100  $\Omega$  sq<sup>-1</sup> (Figure 8A).<sup>[64a]</sup> The reduction in the sheet resistance is attributed to the flowing and partial decomposition of PVP which then allows the Ag NWs to come into contact and fuse together. Continued annealing for more than 40 min led to a gradual increase in sheet resistance as the nanowires break into disconnected droplets.

Sheet resistance of Ag NW films can also be improved by mechanical pressing.<sup>[48,69]</sup> By sandwiching the nanowire networks between two rigid substrates, and applying 81 GPa of pressure for 50 s with a mechanical shop press, Cui and co-workers found the sheet resistance decreased from hundreds of  $\Omega$  sq<sup>-1</sup> to tens of  $\Omega$  sq<sup>-1</sup>.<sup>[48]</sup> Tokuno et al. demonstrated that mechanical pressing at 25 MPa for 5 s at room temperature

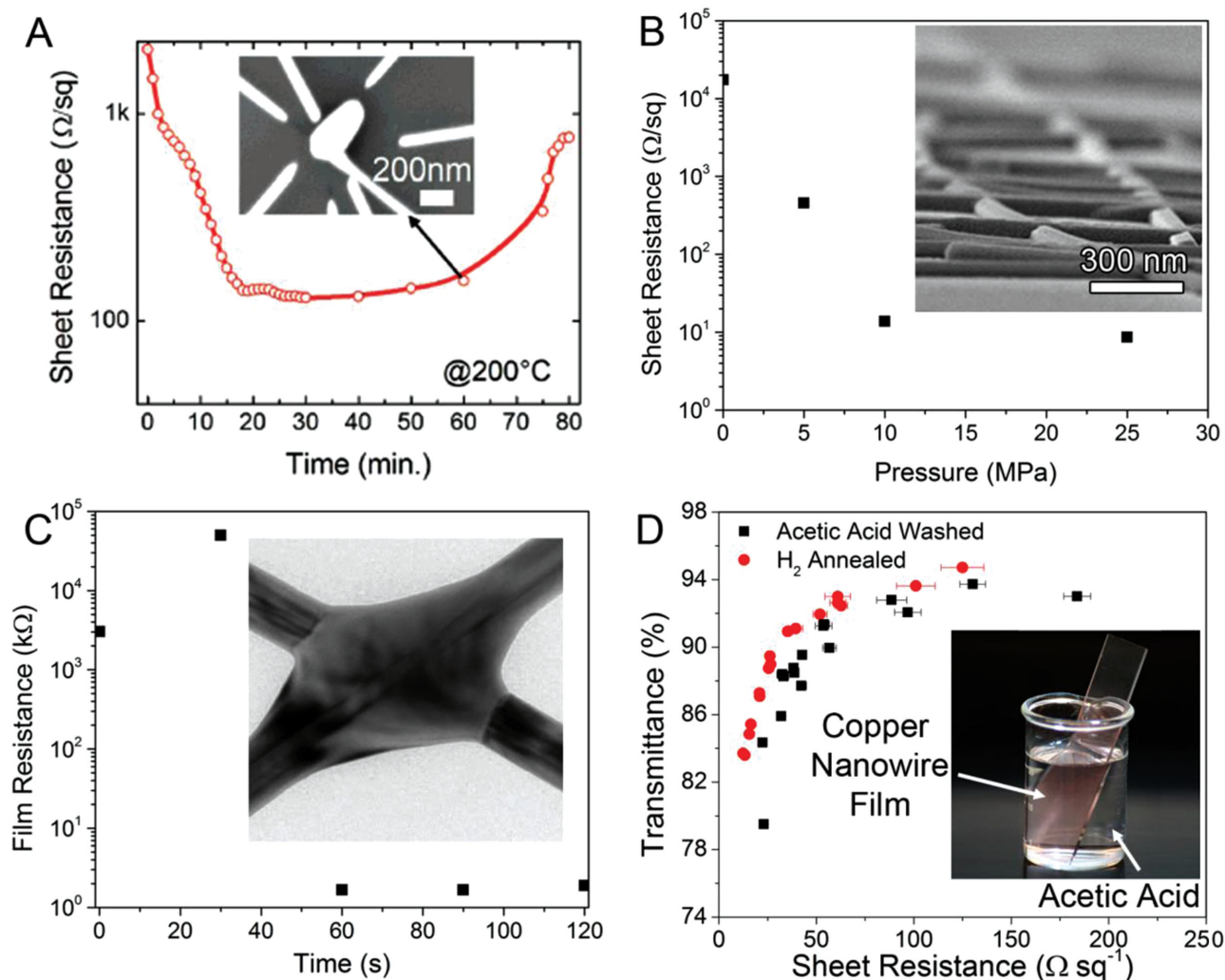


**Figure 8.** A) Thermal annealing at 200 °C initially decreases the sheet resistance of a Ag NW network. The sheet resistance subsequently rises due to melting of the Ag NWs, as shown by the SEM inset. Reproduced with permission.<sup>[64a]</sup> Copyright 2008, American Chemical Society. B) Effect of mechanical pressing on the sheet resistance of a Ag NW film. Inset shows Ag NWs pressed at 25 MPa for 5 s. Reproduced with permission.<sup>[69]</sup> Copyright 2011, Springer. C) Plasmonic welding lowers the sheet resistance of a Ag NW film after 60 s. Inset shows a TEM image of a Ag NW junction after welding. Reproduced with permission.<sup>[47]</sup> Copyright 2012, Macmillan Publishers. D) Acetic acid removes oxides from the surface of Cu NWs, making the films as conductive as annealing in H<sub>2</sub>. Inset shows a Cu NW film immersed in glacial acetic acid. Reproduced with permission.<sup>[62b]</sup> Copyright 2014, Royal Society of Chemistry.



can improve the electrical conductivity of the Ag NW electrodes to be equivalent to those annealed at 200 °C, which makes it possible to fabricate nanowire-based transparent electrodes on heat-sensitive substrates (Figure 8B).<sup>[69]</sup>

Opto-thermal heating techniques have been developed in an effort to quickly reduce the sheet resistance of a nanowire network.<sup>[47]</sup> Exposure of a Ag NW film to a tungsten-halogen lamp at a power density of 30 W cm<sup>-2</sup> for 1 minute welds Ag NWs together and decreases the resistance of the film by three orders of magnitude (Figure 8C). It is thought that the concentration of the incident electromagnetic field in the nanoscale gaps between Ag NWs results in heating only at the point where nanowires need to be joined, preventing damage to the substrate. Other authors have demonstrated that high-intensity pulsed light sources, such as 230 W xenon lamps, can reduce the sheet resistance of a film in 50 μs.<sup>[68a,70]</sup> Such fast processing times may be useful for high-speed roll-to-roll processing.

It has been more difficult to reduce the contact resistance between Cu NWs due to their tendency to oxidize in air. In order to lower the sheet resistance of Cu NW films coated from a nitrocellulose-based ink formulation, the films were placed in a plasma cleaner under a forming gas atmosphere (5% H<sub>2</sub>, 95% N<sub>2</sub>) to remove as much nitrocellulose, PVP and other organics as possible.<sup>[24d]</sup> After plasma cleaning, the films were placed in a tube furnace with a pure hydrogen atmosphere at 175 °C. Since nitrocellulose has a low autoignition temperature, the remaining nitrocellulose vaporized and left a highly conductive Cu NW network. The pure hydrogen gas environment is necessary to reduce the oxide on the surface of Cu NWs and anneal the nanowires together; heating in a forming gas or inert atmosphere does not lower the sheet resistance as much as pure hydrogen. Such hydrogen-based annealing is impractical and has been a hurdle to the wider use of Cu NWs.

It has recently been shown that dipping in acetic acid can make Cu NW films as conductive as annealing in a hydrogen atmosphere (Figure 8D).<sup>[62b,71]</sup> This acid treatment removes the oxides on the surface of Cu NWs as well as the nitrocellulose. One can imagine that a modified version of acetic acid wash can be used to render Cu NW films conductive during roll-to-roll processing.

## 5.2. Decreasing Surface Roughness

The fact that ITO presents a smooth (rms roughness ≈ 2.5–3 nm),<sup>[72]</sup> continuous surface makes it compatible with thin organic electronic devices, such as OLEDs and OPVs. In contrast, nanowire surfaces are not continuous, and as-coated nanowire films typically have surface roughness of at least two nanowire diameters (top-to-bottom roughness ≈ 200–300 nm when the diameter of the nanowires is in between 50 and 100 nm).<sup>[72b]</sup> Such a large roughness is on the order of the thickness of an OLED or OPV, and devices made with rough nanowire films often exhibit short circuits. There are several ways to address the issue of surface roughness for NW films. One is mechanical pressing, which can reduce the average surface roughness of a nanowire film from two diameters (78 nm) to one diameter (37 nm).<sup>[62b]</sup> A second approach is to embed

the nanowires at the surface of a polymer film. For example, Yu et al. coated a Ag NW network with a UV-curable polymer.<sup>[64g]</sup> After curing, the polymer was peeled away to reveal the Ag NWs embedded in its surface. The average surface roughness of the Ag NW/polyacrylate composite electrode was less than 5 nm. Using a slightly different approach, Gaynor et al. transferred a Ag NW film into the surface of a PEDOT:PSS film through the application of pressure to obtain electrodes with an rms roughness as low as 12 nm.<sup>[72b]</sup> Note that it is difficult to achieve reproducible results with such a transfer step. Stewart et al. used mechanical pressing, followed by multiple overcoats of PEDOT:PSS, to achieve an average surface roughness of 18 nm for CuNi nanowire films, and used these films as the anode in an OPV to achieve efficiencies of 4.9%.<sup>[62b]</sup>

## 5.3. Improving Adhesion of Nanowires to the Substrate

Metal nanowires can be easily wiped off a substrate onto which they are coated if no effort is made to adhere them to the substrate. Embedding the nanowires into the surface of a polymer matrix provides one way to improve adhesion, as well as decrease surface roughness, but involves the transfer of nanowires from one substrate to another.<sup>[64g,72b,73]</sup> Akter and Kim demonstrated that the adhesion of Ag NWs to PDMS could be improved by coating the PDMS with polydopamine prior to spray-coating the Ag NWs.<sup>[25e]</sup> The Ag NW film remained on the substrate after a tape peel test.<sup>[25e]</sup> Jin et al. adapted their approach to mix polydopamine and alginate acid into the Ag NW dispersion, and spray-coated this mixture onto PET substrate.<sup>[74]</sup> The resultant Ag NW TC film exhibits a sheet resistance of ca. 16 Ω sq<sup>-1</sup> at 89%T (λ = 550 nm) without the need of high-temperature annealing. The sheet resistance increased by a factor of three after 100 cycles of tape tests, indicating that the Ag NWs adhered well to the substrate. Zilberberg et al. applied a layer of tin oxide (SnO<sub>x</sub>) via a sol-gel process on top of spin-coated Ag NW films.<sup>[75]</sup> Coating of SnO<sub>x</sub> led to a decrease in the sheet resistance from 90 to 5.2 Ω sq<sup>-1</sup>, and a decrease in the %T from 79 to 72 at 632.8 nm. The rms roughness of the composite TC film was reduced from 65 to 34 nm after the SnO<sub>x</sub> coating. The sheet resistance remained unchanged after a tape peel test, or after exposure to 80 °C/80% relative humidity (RH) for a week.

## 5.4. Protection from Corrosion

Both Cu NWs and Ag NWs require protection from atmospheric corrosion. Atmospheric sulfides will react with Ag, converting it into Ag<sub>2</sub>S, which is much less conductive and has a greater absorption cross-section.<sup>[76]</sup> There are several publications on the protection of silver nanostructures from reacting with atmospheric sulfides in order to prolong their ability to serve as substrates for surface enhanced Raman sensing.<sup>[77]</sup> There are also at least two patents on the protection of Ag NWs in the context of TC films,<sup>[76a,78]</sup> but no published academic studies. Given their increasing importance, the protection of Ag NW based TC films from atmospheric corrosion warrants further study.

Unlike Ag, Cu reacts with oxygen at ambient conditions, and thus oxidizes and becomes non-conductive more quickly. Cui and co-workers utilized atomic layer deposition (ALD) to coat a layer of aluminum-doped zinc oxide (AZO) and aluminum oxide ( $\text{Al}_2\text{O}_3$ ) onto electrospun Cu nanofibers in order to prevent their oxidation (Figure 9A).<sup>[79]</sup> After ALD, Cu nanofibers retained the same  $R_s$  and their %T dropped by only 1%. Cu nanofibers coated with the AZO/ $\text{Al}_2\text{O}_3$  layer exhibited a sheet resistance increase of only 10% after heating at 160 °C for 8 hrs in dry air, or after 80 min at 80 °C/80% RH; Cu nanofibers became insulating in less than 40 min under either of these conditions (Figure 9B). This work showed that it is possible to protect a Cu nanofiber network from oxidation without degrading its properties, but the ALD process will likely need to be replaced with a process that is less expensive for such an approach to be practical.

Coating Cu NWs with Ni is an alternative approach to make them highly resistant to oxidation. Rathmell et al. recently reported a solution phase synthesis of CuNi NWs with several Cu to Ni ratios.<sup>[62a]</sup> CuNi NWs were synthesized by reducing Ni onto the surface of Cu NWs with  $\text{N}_2\text{H}_4$ , leading to a core-shell structure (Figure 9C inset). Coating Cu NWs with Ni results in a lower film transmittance at a given sheet resistance due to the increase in the diameter of the nanowires, but it greatly improves their resistance to oxidation. Without any nickel coating, the sheet resistance of the Cu NW films began to increase after 1 day in a dry oven at 85 °C, and increased by an order of magnitude after 5 days (Figure 9C). The sheet resistance of Ag NW films increased by an order of magnitude after 13 days. In comparison, with as little as 10% nickel relative to copper (9:1 Cu:Ni), the sheet resistance of the cupronickel nanowire film remained remarkably stable over a period

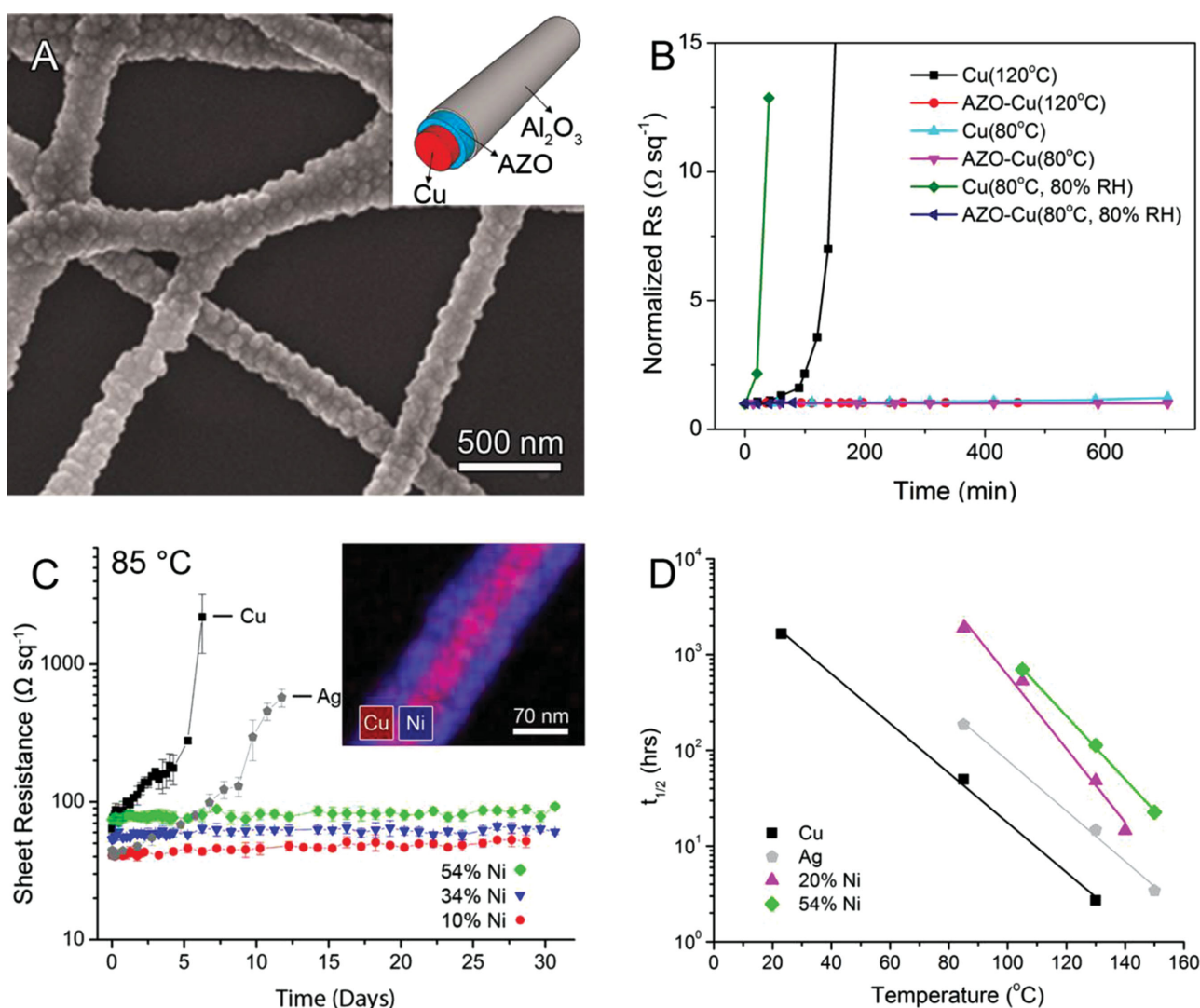


**Figure 9.** A) Cu nanofibers coated with AZO and  $\text{Al}_2\text{O}_3$  via ALD. B) A plot of sheet resistance vs time for Cu and AZO-Cu nanofibers at various oxidation conditions. Reproduced with permission.<sup>[79]</sup> Copyright 2012, American Chemical Society. C) Plot of sheet resistance vs time for films of Ag NWs, Cu NWs, and cupronickel nanowires stored at 85 °C. Inset is an EDS mapping image of a cupronickel nanowire coated with 54 mol% nickel. D) Modified Arrhenius plot of the time required for the sheet resistance to double vs temperature for films of Cu, Ag, 20% Ni, and 54% Ni NWs. Reproduced with permission.<sup>[62a]</sup> Copyright 2012, American Chemical Society.

of 30 days, increasing by only  $10 \Omega \text{ sq}^{-1}$  (from 30 to  $40 \Omega \text{ sq}^{-1}$ ). With Ni contents of 34% or greater, the change in the sheet resistance over 30 days is within the error of the measurement. Based on the temperature-dependent oxidation kinetics (Figure 9D), the times for the sheet resistance of the NW films to double ( $\Delta R/R_0 = 1$ ) at  $25^\circ \text{C}$  are estimated to be 0.2, 3, 400, and 1000 years for networks of copper, silver, 20% Ni, and 54% Ni nanowires, respectively. Subsequent work showed that Ni can also be coated onto the Cu NW films after film formation, and that the resulting films are as stable as Ag NW films under both dry and humid ( $85^\circ \text{C}/85\% \text{ RH}$ ) conditions.<sup>[62b]</sup>

## 6. Device Integration

### 6.1. Touch Screens

The large (ca. \$500 billion) and rapidly growing market for devices that operate through touch-based interfaces represents the most important commercial opportunity for metal nanowires.<sup>[80]</sup> Projected capacitive touch screens, found in nearly all smart phones and tablets, use 6–12 times more ITO than LCD's because of the lower sheet resistance of the ITO in the touch screen, and the fact that there are two TC layers in touch screen versus one in an LCD. Due to the large size and highly competitive nature of the touch module market, there is a strong driving force to lower the cost of touch modules. The lower costs of solution-based metal nanowire coating processes relative to vacuum-based ITO deposition is one way for suppliers of touch modules, and ultimately the suppliers of touch-based devices, to lower the costs of their products. The greater mechanical durability and flexibility of metal nanowire films is a secondary benefit of switching from ITO, and presents an opportunity to develop flexible touch-based devices that would not otherwise be possible due to the brittleness of ITO.<sup>[51]</sup> For example, Lee et al. fabricated a AgNWs/PEDOT:PSS based flexible touch panel that could operate when wrapped around a human arm.<sup>[81]</sup>

Cambrios Technologies and its commercial partners have overcome multiple technical hurdles to introduce the first Ag NW based touch sensors for smart phones,<sup>[82]</sup> desktops,<sup>[83]</sup> and tablets (Figure 10A).<sup>[84]</sup> Besides enabling lower processing costs and greater mechanical flexibility, Ag NWs from Cambrios allow the creation of films with a performance higher than ITO ( $98\%T$  at  $40 \Omega \text{ sq}^{-1}$ ).<sup>[21]</sup> Given these multiple advantages and the success to date, it seems likely that Ag NWs will gain a greater market share of the PET-film based touch sensor market.

### 6.2. Solar Cells

The power-conversion efficiency of OPVs has reached a new record of 11.1%, demonstrating the promise of OPVs as a low-cost alternative to silicon for solar energy harvesting.<sup>[86]</sup> However, it has been noted that a solar energy conversion system cannot cost much more than approximately 10 times the cost of paint ( $\$1 \text{ m}^{-2}$ ), if it is to be cost-competitive with fossil fuels.<sup>[87]</sup> As we noted in the introduction, ITO already costs more than 10 times the cost of paint, and yet can only represent a fraction

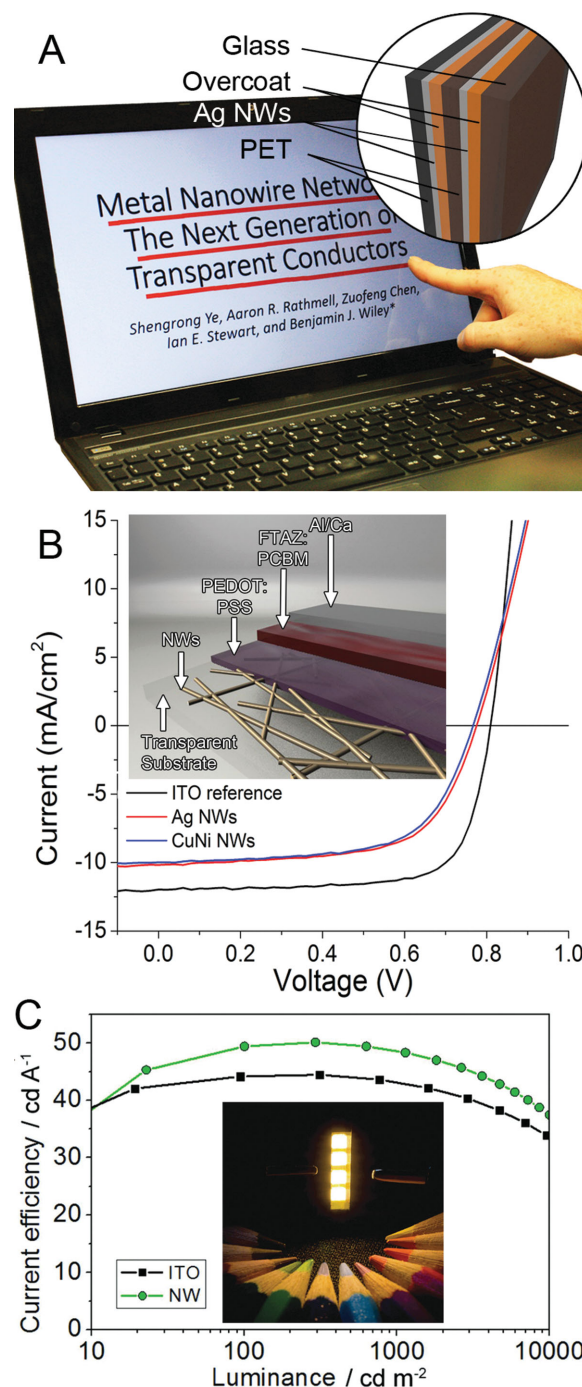


**Figure 10.** A) An example commercial touch panel using Cambrios' ClearOhm Ag NWs.<sup>[21]</sup> B) Characteristic  $J$ - $V$  curves of solar cells with ITO, Ag NWs, and CuNi NWs as the transparent electrode. Inset shows the diagram of the nanowire-based FTAZ-PCBM BHJ solar cell. Reproduced with permission.<sup>[62b]</sup> Copyright 2014, Royal Society of Chemistry. C) Current efficiency of the white OLEDs with nanowire-based and ITO anodes. Inset shows photographic image of four operating nanowire-based OLEDs. Reproduced with permission.<sup>[85]</sup> Copyright 2013, Wiley-VCH.

of the cost of an organic solar cell. Therefore, ITO must be replaced with transparent conducting paint for organic solar cells to ever represent a low cost path to solar energy harvesting.



Initial attempts to replace ITO in OPVs with Ag NW networks resulted in relatively low power conversion efficiencies, from 0.63% to 2.8%.<sup>[64b,64h,67b]</sup> The principle cause of these low efficiencies has been attributed to the fact that the roughness of nanowire networks is on the order of the thickness of a typical polymer active layer.<sup>[72b]</sup> As a result, many of the OPV devices made with nanowire electrodes have exhibited small shunt resistances, and correspondingly low OPV efficiencies.<sup>[64a,64b,66f,67b,88]</sup> This effect of surface roughness on device efficiency has motivated a number of the approaches described in Section 5.2. Embedding the Ag NWs in a polymer surface to give an rms roughness <5 nm resulted in a device efficiency of 3.3%.<sup>[88]</sup> Lamination of Ag NWs into the surface of a PEDOT:PSS layer to give a surface with an rms roughness of 12 nm resulted in a device efficiency of 4.2%.<sup>[72b]</sup> More recently, mechanical pressing followed by multiple overcoats of PEDOT:PSS was used to achieve an OPV efficiency of 5%, even though the %T of the Ag NW film in this case was fairly low (%T = 76,  $R_s = 14 \Omega \text{ sq}^{-1}$ ) relative to ITO.<sup>[62b]</sup> Song et al. have achieved the highest device efficiency to date for Ag NW electrodes (5.8% vs 6.7% on ITO), but surprisingly required no additional smoothing procedures to achieve this device efficiency.<sup>[22]</sup> This may be due to the fact that the diameter of the nanowires,  $25 \pm 5$  nm, and the corresponding rms roughness of the as-coated Ag NW film (13 nm) was small enough that did not negatively impact the efficiency of the device. The relatively high efficiency of the device in this case was principally due to the high performance ( $10 \Omega \text{ sq}^{-1}$  at 95%T) of the Ag NW film-based electrodes.

In comparison to the many studies on the replacement of ITO in OPVs with Ag NWs, only two articles have been published on the replacement of ITO with solution-coated films of Cu NWs.<sup>[62b,89]</sup> This is likely due to the challenges associated with making Cu NW networks conductive and protecting them from oxidation. In the first study on replacement of ITO in OPVs with Cu NWs, the Cu NW film was annealed in hydrogen to make it conductive, and planarized with PEDOT:PSS.<sup>[89]</sup> The authors noted that the processing conditions had to be modified to prevent the degradation of the Cu NW film during coating of the acidic PEDOT:PSS suspension. The authors vacuum deposited the remaining layers onto this anode to create a bulk-heterojunction (BHJ) small-molecule organic solar cell with an efficiency of 3%. Subsequent work by Stewart et al. demonstrated an all solution-phase process to replace ITO with Cu NWs in an OPV.<sup>[62b]</sup> After coating Cu NWs from an ink onto glass, the films were made conductive by dipping them in acetic acid, and protected from oxidation by dipping them in a Ni electroless plating solution. CuNi NW films were then integrated into a solution-coated OPV to give a device efficiency of 4.9% (Figure 10B), compared to 7.1% for ITO. The lower efficiency of the CuNi device was attributed to the lower transmittance of the CuNi film at the same sheet resistance. Further improvements in the optoelectronic performance of passivated Cu NW films will likely yield device efficiencies comparable to those obtained using ITO.

### 6.3. OLEDs

A high-performance, low-cost transparent conductor is a critical component for large area OLEDs. High sheet resistance will

increase the operating voltage, resistive heating, non-uniform emission, and differential aging across the device, whereas low optical transparency will reduce the external quantum efficiency.<sup>[64a,64b,85]</sup> The transparent conductor substrate should also be flexible to make it compatible for low-cost, roll-to-roll production of OLEDs for lighting. Researchers are motivated to replace the use of ITO for OLEDs not only because of its high cost, but also because the sheet resistance of ITO on flexible PET substrates is about 5 times higher ( $50 \Omega \text{ sq}^{-1}$ ) than on glass due to the lower temperatures used for deposition of ITO onto plastic. The low cost and high performance of metal nanowire films on plastic substrates makes them a promising alternative to ITO as the transparent electrode for OLEDs, but first the nanowire electrodes must be made to be nearly as smooth as ITO. In one case, researchers coated a Ag NW network with a UV-curable polymer, and after curing peeled the polymer away to reveal a smooth Ag NW electrode.<sup>[64g]</sup> The efficiency of devices made with the Ag NW electrode were as high as  $14.0 \text{ cd A}^{-1}$ , which was slightly higher than the control devices using an ITO anode.<sup>[64g]</sup> Gaynor et al. made smooth Ag NW anodes by coating a transparent substrate with poly(methyl methacrylate) (PMMA), spray-coating Ag NWs onto the PMMA-coated substrate, and pressing the Ag NWs into the PMMA while heating the substrate.<sup>[85]</sup> The current efficiency of white OLEDs fabricated on these electrodes was higher than the same OLEDs on ITO (Figure 10C). The nanowire anode also improved the angular color stability of the OLED relative to ITO due to its relatively greater haze.

## 7. Conclusion and Outlook

While ITO has been the most widely used transparent conductor for decades, and will likely continue to play that role well into the future, metal nanowires represent the first alternative to ITO that can be coated from solution and achieve optoelectronic performance that exceeds that of ITO. Given that most of the production cost of a highly conductive ( $10 \Omega \text{ sq}^{-1}$ ) ITO film arises from the vapor-phase sputtering process, the availability of a high-performance, solution-coatable alternative could enable dramatic reductions in the price of highly conductive, transparent films. Lower cost TC films will in turn enable the production of lower-cost touch-screens, OLEDs and OPVs.

Given the potential importance of metal nanowire-based TCs for a range of applications, it is important to understand how to optimize the properties of a nanowire-based transparent electrode. We have discussed how the resistivity, optical cross-section, areal density, aspect ratio, and contact resistance of metal nanowires influence the properties of metal nanowire films. Current models for the properties of nanowire films may be improved by the inclusion of the resistance of the nanowires, as well as the fact that nanowires tend to become more curved and wavy as their aspect ratio increases. Efforts to increase the aspect ratio of synthesized nanowires, and thereby improve the performance of nanowire-based TC films, have to date achieved  $L/D = 600$  for Ag NWs, and 2500 for Cu NWs. Additional performance improvements may be achieved through the synthesis of high aspect ratio nanowires with smaller diameters ( $D < 25 \text{ nm}$ ), which will scatter less light. As both experimental

and modeling results show that the contact resistance between nanowires dominates the sheet resistance of a nanowire network, it is also important to understand why this is the case, and how to reduce the contact resistance between nanowires to be close to the resistance of a nanowire. Finally, it is clear that different types of devices may require different densities of nanowires, or may benefit from the use of nanowires with a particular dimension. For example, whereas haze should be minimized for a touch screen, haze may be desirable in the case of an OPV. Further study is needed to better understand how we can control the structure and properties of a nanowire-based TC to optimize the properties for a particular class of devices.

## Acknowledgements

This work was supported by NSF's Research Triangle MRSEC (DMR-1121107), and an NSF CAREER award (DMR-1253534). I.E.S. was supported by a fellowship through the Duke graduate program in nanoscience.

Received: June 17, 2014  
Published online:

- [1] Indium Tin Oxide and Alternative Transparent Conductor Markets, NanoMarkets, LC, **2009**.
- [2] K. Ghaffarzadeh, R. Das, *Transparent Conductive Films (TCF)*, Forecasts, Markets, Technologies (IDTechEx), pp. 2014–2024.
- [3] D. S. Hecht, L. Hu, G. Irvin, *Adv. Mater.* **2011**, *23*, 1482–1513.
- [4] U.S. Geological Survey, *Mineral Commodity Summaries, Indium*, U.S. Department of the Interior, Washington, D.C., USA **2014**, p. 74.
- [5] The cost of ITO/PET films was provided by the Kintec Company of Hongkong, China (<http://www.kintec.hk/>). For ITO-PET films with sheet resistances/ thicknesses of  $10 \Omega \text{ sq}^{-1}/180 \text{ nm}$ ,  $20 \Omega \text{ sq}^{-1}/100 \text{ nm}$ ,  $25 \Omega \text{ sq}^{-1}/85 \text{ nm}$ ,  $50 \Omega \text{ sq}^{-1}/35 \text{ nm}$ ,  $80 \Omega \text{ sq}^{-1}/30 \text{ nm}$ ,  $100 \Omega \text{ sq}^{-1}/25 \text{ nm}$ , and  $150 \Omega \text{ sq}^{-1}/20 \text{ nm}$ , their corresponding prices are \$26, 17, 15, 13, 7, 6.5, and 5.5 per  $\text{m}^2$ , respectively. The cost of PET film itself is \$3–4 per  $\text{m}^2$ . For a 100 nm-thick film of ITO, which contains  $0.53 \text{ g In m}^{-2}$  [ $100 \text{ nm (thickness)} \times 7140 \text{ kg m}^{-3}$  (ITO density)  $\times 90\%$  (mass percent of  $\text{In}_2\text{O}_3$  in ITO)  $\times 82.7\%$  (atomic weight of In in  $\text{In}_2\text{O}_3$ )] that costs  $\$0.32 \text{ m}^{-2}$  ( $0.53 \text{ g In m}^{-2} \times \$600 \text{ kg}^{-1}$ ), approximately 2.2% of the film cost can be contributed to the cost of indium [ $\$0.32 \text{ m}^{-2}/(\$17\text{--}\$3)$ ].
- [6] B. Azzopardi, C. J. M. Emmott, A. Urbina, F. C. Krebs, J. Mutale, J. Nelson, *Energy Environ. Sci.* **2011**, *4*, 3741–3753.
- [7] C. J. Brabec, J. R. Durrant, *MRS Bull.* **2008**, *33*, 670–675.
- [8] K. Zweibel, *Sol. Energy Mater. Sol. Cells* **1999**, *59*, 1–18.
- [9] a) F. C. Krebs, *Sol. Energy Mater. Sol. Cells* **2009**, *93*, 465–475; b) S.-I. Na, S.-S. Kim, J. Jo, D.-Y. Kim, *Adv. Mater.* **2008**, *20*, 4061–4067.
- [10] A. Elschner, W. Lövenich, *MRS Bull.* **2011**, *36*, 794–798.
- [11] a) Heraeus Clevios Conductive Polymers website, <http://www.heraeus-clevios.com/>, accessed: **August 2014**; b) AGFA Orgacon Materials website, <https://www.agfa.com/>, accessed: **August 2014**.
- [12] a) C. Niu, *MRS Bull.* **2011**, *36*, 766–773; b) Z. Wu, Z. Chen, X. Du, J. M. Logan, J. Sippel, M. Nikolou, K. Kamaras, J. R. Reynolds, D. B. Tanner, A. F. Hebard, A. G. Rinzier, *Science* **2004**, *305*, 1273–1276; c) D. S. Hecht, A. M. Heintz, R. Lee, L. Hu, B. Moore, C. Cucksey, S. Risser, *Nanotechnology* **2011**, *22*, 075201.
- [13] H.-Z. Geng, K. K. Kim, K. P. So, Y. S. Lee, Y. Chang, Y. H. Lee, *J. Am. Chem. Soc.* **2007**, *129*, 7758–7759.
- [14] S. Bae, H. Kim, Y. Lee, X. Xu, J.-S. Park, Y. Zheng, J. Balakrishnan, T. Lei, H. Ri Kim, Y. I. Song, Y.-J. Kim, K. S. Kim, B. Ozyilmaz, J.-H. Ahn, B. H. Hong, S. Iijima, *Nat. Nanotechnol.* **2010**, *5*, 574–578.
- [15] J. H. Lee, D. W. Shin, V. G. Makotchenko, A. S. Nazarov, V. E. Fedorov, Y. H. Kim, J.-Y. Choi, J. M. Kim, J.-B. Yoo, *Adv. Mater.* **2009**, *21*, 4383–4387.
- [16] R. A. Hatton, M. R. Willis, M. A. Chesters, D. Briggs, *J. Mater. Chem.* **2003**, *13*, 722–726.
- [17] N. Formica, D. Sundar Ghosh, T. L. Chen, C. Eickhoff, I. Bruder, V. Pruneri, *Sol. Energy Mater. Sol. Cells* **2012**, *107*, 63–68.
- [18] a) UniPixel, Inc. website, <http://www.unipixel.com/>, accessed: **August 2014**; b) 3M website, <http://www.3m.com/>, accessed: **August 2014**; c) PolyIC GmbH & Co. KG website, <http://www.polyic.com/>, accessed: **August 2014**; d) Kodak website, <http://www.kodak.com/>, accessed: **August 2014**; e) Atmel Corporation website, <http://www.atmel.com/>, accessed: **August 2014**; f) O-film Tech. Co. Ltd. website, <http://www.o-film.com/>, accessed: **August 2014**.
- [19] Rolith, Inc. website, <http://www.rolith.com/applications/transparent-conductive-electrodes>, accessed: **August 2014**.
- [20] a) J. Woerle, H. Rost, *MRS Bull.* **2011**, *36*, 789–793; b) M. G. Kang, L. J. Guo, *Adv. Mater.* **2007**, *19*, 1391–1396.
- [21] Cambrios Technologies, <http://www.cambrios.com/>, accessed: **August 2014**.
- [22] M. Song, D. S. You, K. Lim, S. Park, S. Jung, C. S. Kim, D.-H. Kim, D.-G. Kim, J.-K. Kim, J. Park, Y.-C. Kang, J. Heo, S.-H. Jin, J. H. Park, J.-W. Kang, *Adv. Funct. Mater.* **2013**, *4177*–4184.
- [23] U.S. Geological Survey, *Mineral Commodity Summaries, Silver*, U.S. Department of the Interior, Washington, D.C., USA **2014**, p. 146.
- [24] a) S. Ye, A. R. Rathmell, I. E. Stewart, Y.-C. Ha, A. R. Wilson, Z. Chen, B. J. Wiley, *Chem. Commun.* **2014**, *50*, 2562–2564; b) A. R. Rathmell, S. M. Bergin, Y.-L. Hua, Z.-Y. Li, B. J. Wiley, *Adv. Mater.* **2010**, *22*, 3558–3563; c) M. Jin, G. He, H. Zhang, J. Zeng, Z. Xie, Y. Xia, *Angew. Chem. Int. Ed.* **2011**, *50*, 10560–10564; d) A. R. Rathmell, B. J. Wiley, *Adv. Mater.* **2011**, *23*, 4798–4803; e) D. Zhang, R. Wang, M. Wen, D. Weng, X. Cui, J. Sun, H. Li, Y. Lu, *J. Am. Chem. Soc.* **2012**, *134*, 14283–14286; f) H. Guo, N. Lin, Y. Chen, Z. Wang, Q. Xie, T. Zheng, N. Gao, S. Li, J. Kang, D. Cai, D.-L. Peng, *Sci. Rep.* **2013**, *3*, 2323.
- [25] a) J. Wu, J. Zang, A. R. Rathmell, X. Zhao, B. J. Wiley, *Nano Lett.* **2013**, *13*, 2381–2386; b) C. Yan, J. Wang, X. Wang, W. Kang, M. Cui, C. Y. Foo, P. S. Lee, *Adv. Mater.* **2014**, *26*, 943–950; c) S. Yao, Y. Zhu, *Nanoscale* **2014**, *6*, 2345–2352; d) M. Amjadi, A. Pichitpajongkit, S. Lee, S. Ryu, I. Park, *ACS Nano* **2014**, *8*, 5154–5163; e) T. Akter, W. S. Kim, *ACS Appl. Mater. Interfaces* **2012**, *4*, 1855–1859; f) X. Ho, J. N. Tey, W. Liu, C. K. Cheng, J. Wei, *J. Appl. Phys.* **2013**, *113*, 044311.
- [26] H. Hagendorfer, K. Lienau, S. Nishiwaki, C. M. Fella, L. Kranz, A. R. Uhl, D. Jaeger, L. Luo, C. Gretener, S. Buecheler, Y. E. Romanyuk, A. N. Tiwari, *Adv. Mater.* **2014**, *26*, 632–636.
- [27] M. Kevin, G. H. Lee, G. W. Ho, *Energy Environ. Sci.* **2012**, *5*, 7196–7202.
- [28] B. O'Connor, C. Haughn, K.-H. An, K. P. Pipe, M. Shtein, *Appl. Phys. Lett.* **2008**, *93*, 223304.
- [29] D. S. Ghosh, L. Martinez, S. Giurgola, P. Vergani, V. Pruneri, *Opt. Lett.* **2009**, *34*, 325–327.
- [30] C. F. Guo, T. Sun, Q. Liu, Z. Suo, Z. Ren, *Nat. Commun.* **2014**, *5*, 3121.
- [31] H. Wu, L. Hu, M. W. Rowell, D. Kong, J. J. Cha, J. R. McDonough, J. Zhu, Y. Yang, M. D. McGehee, Y. Cui, *Nano Lett.* **2010**, *10*, 4242–4248.
- [32] F. Mirri, A. W. K. Ma, T. T. Hsu, N. Behabtu, S. L. Eichmann, C. C. Young, D. E. Tsentelovich, M. Pasquali, *ACS Nano* **2012**, *6*, 9737–9744.

- [33] G. Eda, G. Fanchini, M. Chhowalla, *Nat. Nanotechnol.* **2008**, *3*, 270–274.
- [34] R. B. Dingle, *Proc. R. Soc. London, A* **1950**, *201*, 545–560.
- [35] K. Fuchs, *Math. Proc. Cambridge* **1938**, *34*, 100–108.
- [36] J. M. Ziman, *Electrons and Phonons*, Clarendon Press, Oxford, UK, **1960**.
- [37] S. B. Soffer, *J. Appl. Phys.* **1967**, *38*, 1710–1715.
- [38] J. R. Sambles, K. C. Elsom, T. W. Preist, *J. Phys. F* **1982**, *12*, 1169.
- [39] M. M. Kole nik, S. Hansel, T. Lutz, N. Kinahan, M. Boese, V. Krstić, *Small* **2011**, *7*, 2873–2877.
- [40] R. L. Graham, G. B. Alers, T. Mountsier, N. Shamma, S. Dhuey, S. Cabrini, R. H. Geiss, D. T. Read, S. Peddeti, *Appl. Phys. Lett.* **2010**, *96*, 042116.
- [41] K. Critchley, B. P. Khanal, M. Ł. Górzny, L. Vigderman, S. D. Evans, E. R. Zubarev, N. A. Kotov, *Adv. Mater.* **2010**, *22*, 2338–2342.
- [42] S. M. Bergin, Y.-H. Chen, A. R. Rathmell, P. Charbonneau, Z.-Y. Li, B. J. Wiley, *Nanoscale* **2012**, *4*, 1996–2004.
- [43] G. Khanarian, J. Joo, X.-Q. Liu, P. Eastman, D. Werner, apos, K. Connell, P. Trefonas, *J. Appl. Phys.* **2013**, *114*, 024302.
- [44] L. Wang, M. R. Kamal, A. D. Rey, *Polym. Eng. Sci.* **2001**, *41*, 358–372.
- [45] a) H. A. Atwater, A. Polman, *Nat. Mater.* **2010**, *9*, 205–213; b) C. Preston, Z. Fang, J. Murray, H. Zhu, J. Dai, J. N. Munday, L. Hu, *J. Mater. Chem. C* **2014**, *2*, 1248–1254.
- [46] G. E. Pike, C. H. Seager, *I. Phys. Rev. B* **1974**, *10*, 1421–1434.
- [47] E. C. Garnett, W. Cai, J. J. Cha, F. Mahmood, S. T. Connor, M. Greyson Christoforo, Y. Cui, M. D. McGehee, M. L. Brongersma, *Nat. Mater.* **2012**, *11*, 241–249.
- [48] L. Hu, H. S. Kim, J.-Y. Lee, P. Peumans, Y. Cui, *ACS Nano* **2010**, *4*, 2955–2963.
- [49] R. M. Mutiso, M. C. Sherrott, A. R. Rathmell, B. J. Wiley, K. I. Winey, *ACS Nano* **2013**, *7*, 7654–7663.
- [50] a) Y. Sun, B. Gates, B. Mayers, Y. Xia, *Nano Lett.* **2002**, *2*, 165–168; b) Y. Sun, Y. Xia, *Adv. Mater.* **2002**, *14*, 833–837; c) Y. Sun, Y. Yin, B. T. Mayers, T. Herricks, Y. Xia, *Chem. Mater.* **2002**, *14*, 4736–4745.
- [51] J. Lee, P. Lee, H. Lee, D. Lee, S. S. Lee, S. H. Ko, *Nanoscale* **2012**, *4*, 6408–6414.
- [52] a) L. D. Marks, *Rep. Prog. Phys.* **1994**, *57*, 603; b) F. Baletto, R. Ferrando, *Rev. Mod. Phys.* **2005**, *77*, 371.
- [53] C. Lofton, W. Sigmund, *Adv. Funct. Mater.* **2005**, *15*, 1197–1208.
- [54] Y. Sun, B. Mayers, T. Herricks, Y. Xia, *Nano Lett.* **2003**, *3*, 955–960.
- [55] B. Wiley, Y. Sun, Y. Xia, *Langmuir* **2005**, *21*, 8077–8080.
- [56] S. E. Skrabalak, B. J. Wiley, M. Kim, E. V. Formo, Y. Xia, *Nano Lett.* **2008**, *8*, 2077–2081.
- [57] K. E. Korte, S. E. Skrabalak, Y. Xia, *J. Mater. Chem.* **2008**, *18*, 437–441.
- [58] Y. Chang, M. L. Lye, H. C. Zeng, *Langmuir* **2005**, *21*, 3746–3748.
- [59] S. Ye, A. R. Rathmell, Y.-C. Ha, A. R. Wilson, B. J. Wiley, *Small* **2014**, *10*, 1771–1778.
- [60] Y. Shi, H. Li, L. Chen, X. Huang, *Sci. Tech. Adv. Mater.* **2005**, *6*, 761.
- [61] M. Mohl, P. Pusztai, A. Kukovecz, Z. Konya, J. Kukkola, K. Kordas, R. Vajtai, P. M. Ajayan, *Langmuir* **2010**, *26*, 16496–16502.
- [62] a) A. R. Rathmell, M. Nguyen, M. Chi, B. J. Wiley, *Nano Lett.* **2012**, *12*, 3193–3199; b) I. E. Stewart, A. R. Rathmell, L. Yan, S. Ye, P. F. Flowers, W. You, B. J. Wiley, *Nanoscale* **2014**, *6*, 5980–5988; c) S. Li, Y. Chen, L. Huang, D. Pan, *Inorg. Chem.* **2014**, *53*, 4440–4444.
- [63] S.-Y. Bae, I.-Y. Jeon, J. Yang, N. Park, H. S. Shin, S. Park, R. S. Ruoff, L. Dai, J.-B. Baek, *ACS Nano* **2011**, *5*, 4974–4980.
- [64] a) J.-Y. Lee, S. T. Connor, Y. Cui, P. Peumans, *Nano Lett.* **2008**, *8*, 689–692; b) W. Gaynor, J.-Y. Lee, P. Peumans, *ACS Nano* **2010**, *4*, 30–34; c) B. E. Hardin, W. Gaynor, I. K. Ding, S.-B. Rim, P. Peumans, M. D. McGehee, *Org. Electron.* **2011**, *12*, 875–879; d) W. Hu, X. Niu, L. Li, S. Yun, Z. Yu, Q. Pei, *Nanotechnology* **2012**, *23*, 344002; e) F. Xu, Y. Zhu, *Adv. Mater.* **2012**, *24*, 5117–5122; f) S. Yun, X. Niu, Z. Yu, W. Hu, P. Brochu, Q. Pei, *Adv. Mater.* **2012**, *24*, 1321–1327; g) Z. Yu, Q. Zhang, L. Li, Q. Chen, X. Niu, J. Liu, Q. Pei, *Adv. Mater.* **2011**, *23*, 664–668; h) J.-Y. Lee, S. T. Connor, Y. Cui, P. Peumans, *Nano Lett.* **2010**, 101276–1279.
- [65] a) S. De, T. M. Higgins, P. E. Lyons, E. M. Doherty, P. N. Nirmalraj, W. J. Blau, J. J. Boland, J. N. Coleman, *ACS Nano* **2009**, *3*, 1767–1774; b) P. Lee, J. Lee, H. Lee, J. Yeo, S. Hong, K. H. Nam, D. Lee, S. S. Lee, S. H. Ko, *Adv. Mater.* **2012**, *24*, 3326–3332; c) P. E. Lyons, S. De, J. Elias, M. Schamel, L. Philippe, A. T. Bellew, J. J. Boland, J. N. Coleman, *J. Phys. Chem. Lett.* **2011**, *2*, 3058–3062.
- [66] a) Y. Ahn, Y. Jeong, Y. Lee, *ACS Appl. Mater. Interfaces* **2012**, *4*, 6410–6414; b) T.-G. Chen, B.-Y. Huang, H.-W. Liu, Y.-Y. Huang, H.-T. Pan, H.-F. Meng, P. Yu, *ACS Appl. Mater. Interfaces* **2012**, *4*, 6857–6864; c) L.-H. Chen, P. Lin, M.-C. Chen, P.-Y. Huang, C. Kim, J.-C. Ho, C.-C. Lee, *Org. Electron.* **2012**, *13*, 1881–1886; d) C.-H. Chung, T.-B. Song, B. Bob, R. Zhu, H.-S. Duan, Y. Yang, *Adv. Mater.* **2012**, *24*, 5499–5504; e) C.-C. Chen, L. Dou, R. Zhu, C.-H. Chung, T.-B. Song, Y. B. Zheng, S. Hawks, G. Li, P. S. Weiss, Y. Yang, *ACS Nano* **2012**, *6*, 7185–7190; f) D.-S. Leem, A. Edwards, M. Faist, J. Nelson, D. D. C. Bradley, J. C. de Mello, *Adv. Mater.* **2011**, *23*, 4371–4375; g) J. Ajuria, I. Ugarte, W. Cambarau, I. Etxebarria, R. Tena-Zaera, R. Pacios, *Sol. Energy Mater. Sol. Cells* **2012**, *102*, 148–152.
- [67] a) C. Celle, C. Mayousse, E. Moreau, H. Basti, A. Carella, J.-P. Simonato, *Nano Res.* **2012**, *5*, 427–433; b) L. Yang, T. Zhang, H. Zhou, S. C. Price, B. J. Wiley, W. You, *ACS Appl. Mater. Interfaces* **2011**, *3*, 4075–4084; c) D. Y. Choi, H. W. Kang, H. J. Sung, S. S. Kim, *Nanoscale* **2013**, *5*, 977–983; d) A. Afal, S. Coskun, H. E. Unalan, *Appl. Phys. Lett.* **2013**, *102*, 043503; e) I. N. Kholmanov, S. H. Domingues, H. Chou, X. Wang, C. Tan, J.-Y. Kim, H. Li, R. Piner, A. J. G. Zarbin, R. S. Ruoff, *ACS Nano* **2013**, *7*, 1811–1816; f) A. R. Madaria, A. Kumar, C. Zhou, *Nanotechnology* **2011**, *22*, 245201; g) V. Scardaci, R. Coull, P. E. Lyons, D. Rickard, J. N. Coleman, *Small* **2011**, *7*, 2621–2628; h) S. Sorel, U. Khan, J. N. Coleman, *Appl. Phys. Lett.* **2012**, *101*, 103106; i) R. Zhu, C.-H. Chung, K. C. Cha, W. Yang, Y. B. Zheng, H. Zhou, T.-B. Song, C.-C. Chen, P. S. Weiss, G. Li, Y. Yang, *ACS Nano* **2011**, *5*, 9877–9882.
- [68] a) J. Jiu, M. Nogi, T. Sugahara, T. Tokuno, T. Araki, N. Komoda, K. Suganuma, H. Uchida, K. Shinozaki, *J. Mater. Chem.* **2012**, *22*, 23561–23567; b) L. Hu, G. Zheng, J. Yao, N. Liu, B. Weil, M. Eskilsson, E. Karabulut, Z. Ruan, S. Fan, J. T. Bloking, M. D. McGehee, L. Wagberg, Y. Cui, *Energy Environ. Sci.* **2013**, *6*, 513–518; c) M. Hu, J. Gao, Y. Dong, K. Li, G. Shan, S. Yang, R. K.-Y. Li, *Langmuir* **2012**, *28*, 7101–7106; d) Z. Chen, A. R. Rathmell, S. Ye, A. R. Wilson, B. J. Wiley, *Angew. Chem. Inter. Ed.* **2013**, *52*, 13708–13711; e) Z. Chen, S. Ye, A. B. Wilson, Y.-C. Ha, B. J. Wiley, *Energy Environ. Sci.* **2014**, *7*, 1461–1467.
- [69] T. Tokuno, M. Nogi, M. Karakawa, J. Jiu, T. Nge, Y. Aso, K. Suganuma, *Nano Res.* **2011**, *4*, 1215–1222.
- [70] a) J. Spechler, C. Arnold, *Appl. Phys. A* **2012**, *108*, 25–28; b) S. Guo, *Nanoscale* **2010**, *2*, 2521–2529; c) J. S. Kang, J. Ryu, H. S. Kim, H. T. Hahn, *J. Electron. Mater.* **2011**, *40*, 2268–2277; d) H.-S. Kim, S. Dhage, D.-E. Shim, H. T. Hahn, *Appl. Phys. A* **2009**, *97*, 791–798; e) J. Ryu, H.-S. Kim, H. T. Hahn, *J. Electron. Mater.* **2011**, *40*, 42–50.
- [71] C. Mayousse, C. Celle, A. Carella, J.-P. Simonato, *Nano Res.* **2014**, *7*, 315–324.
- [72] a) Y. Yang, Q. Huang, A. W. Metz, J. Ni, S. Jin, T. J. Marks, M. E. Madsen, A. DiVenere, S. T. Ho, *Adv. Mater.* **2004**, *16*, 321–324; b) W. Gaynor, G. F. Burkhard, M. D. McGehee, P. Peumans, *Adv. Mater.* **2011**, *23*, 2905–2910.
- [73] M. S. Miller, J. C. O’Kane, A. Niec, R. S. Carmichael, T. B. Carmichael, *ACS Appl. Mater. Interfaces* **2013**, *5*, 10165–10172.
- [74] Y. Jin, D. Deng, Y. Cheng, L. Kong, F. Xiao, *Nanoscale* **2014**, *6*, 4812–4818.



- [75] K. Zilberberg, F. Gasse, R. Pagui, A. Polywka, A. Behrendt, S. Trost, R. Heiderhoff, P. Görrn, T. Riedl, *Adv. Funct. Mater.* **2014**, *24*, 1671–1678.
- [76] a) P.-M. Allemand, H. Dai, S. Na, H. Pakbaz, F. Pschenitzka, X. Quan, J. Sepa, M. A. Spaid, (Cambrios Technologies Corporation, USA), *US 2008/0143906 A1*, **2008**; b) J. L. Elechiguerra, L. Larios-Lopez, C. Liu, D. Garcia-Gutierrez, A. Camacho-Bragado, M. J. Yacamán, *Chem. Mater.* **2005**, *17*, 6042–6052.
- [77] a) Y. Yang, J. Liu, Z.-W. Fu, D. Qin, *J. Am. Chem. Soc.* **2014**, *136*, 8153–8156; b) C. Gao, Z. Lu, Y. Liu, Q. Zhang, M. Chi, Q. Cheng, Y. Yin, *Angew. Chem. Int. Ed.* **2012**, *51*, 5629–5633; c) M. M. Shahjamali, M. Bosman, S. Cao, X. Huang, S. Saadat, E. Martinsson, D. Aili, Y. Y. Tay, B. Liedberg, S. C. J. Loo, H. Zhang, F. Boey, C. Xue, *Adv. Funct. Mater.* **2012**, *22*, 849–854; d) N. Murshid, I. Gourevich, N. Coombs, V. Kitaev, *Chem. Commun.* **2013**, *49*, 11355–11357.
- [78] C. Zou, R. William, (Carestream Health, Inc., USA), *US 2013/0004765 A1*, 2013.
- [79] P.-C. Hsu, H. Wu, T. J. Carney, M. T. McDowell, Y. Yang, E. C. Garnett, M. Li, L. Hu, Y. Cui, *ACS Nano* **2012**, *6*, 5150–5156.
- [80] a) Fundamentals of projected-capacitive touch technology; [http://www.walkermobile.com/Touch\\_Technologies\\_Tutorial\\_Latest\\_Version.pdf](http://www.walkermobile.com/Touch_Technologies_Tutorial_Latest_Version.pdf), accessed: **August 2014**; b) The \$750 billion converged living room: a plateau approaches; [http://www2.deloitte.com/content/dam/Deloitte/global/Documents/Technology-Media-Telecommunications/gx-tmt-2014prediction-\\$750-billion.pdf](http://www2.deloitte.com/content/dam/Deloitte/global/Documents/Technology-Media-Telecommunications/gx-tmt-2014prediction-$750-billion.pdf), accessed: **August 2014**.
- [81] J. Lee, P. Lee, H. B. Lee, S. Hong, I. Lee, J. Yeo, S. S. Lee, T.-S. Kim, D. Lee, S. H. Ko, *Adv. Funct. Mater.* **2013**, *23*, 4171–4176.
- [82] Cambrios ClearOhm film used in smart phone, 2011, <http://www.printedelectronicsworld.com/articles/cambrios-clearohm-film-used-in-smart-phone-00003279.asp?sessionid=1>, accessed: **August 2014**.
- [83] Cambrios and LG Electronics Announce World's First 23" Touch Panels Using ClearOhm Material, 2012, <http://www.reuters.com/article/2012/10/31/idUS10004+31-Oct-2012+BW20121031>, accessed: **August 2014**.
- [84] Cambrios' ClearOhm to Deliver Advanced Touchscreen Experience for Lenovo Flex 20, 2013, <http://www.cambrios.com/news/cambrios%E2%80%99-clearohm%C2%AE-deliver-advanced-touchscreen-experience-lenovo-flex-20>, accessed: **August 2014**.
- [85] W. Gaynor, S. Hofmann, M. G. Christoforo, C. Sachse, S. Mehra, A. Salleo, M. D. McGehee, M. C. Gather, B. Lüssem, L. Müller-Meskamp, P. Peumans, K. Leo, *Adv. Mater.* **2013**, *25*, 4006–4013.
- [86] NREL chart on record cell efficiencies. <http://www.nrel.gov/ncpv/>, accessed: **August 2014**.
- [87] a) N. S. Lewis, D. G. Nocera, *Proc. Natl. Acad. Sci. USA* **2006**, *103*, 15729–15735; b) C. Wadia, A. P. Alivisatos, D. M. Kammen, *Environ. Sci. Technol.* **2009**, *43*, 2072–2077.
- [88] Z. Yu, L. Li, Q. Zhang, W. Hu, Q. Pei, *Adv. Mater.* **2011**, *23*, 4453–4457.
- [89] C. Sachse, N. Weiß, N. Gaponik, L. Müller-Meskamp, A. Eychmüller, K. Leo, *Adv. Energy Mater.* **2014**, *4*, 1300737.